DOE/EE--97000108
June 1993

Assessment of Strength-Limiting Flaws in Ceramic Heat Exchanger Components

INEL Support: Fracture Mechanics and Nondestructive Evaluation Technology - Final Report

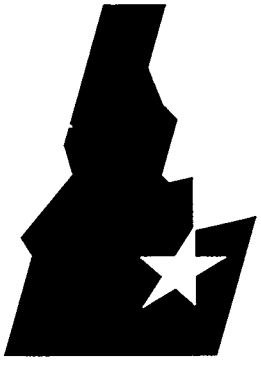

Idaho National Engineering Laboratory

U.S. Department of Energy • Idaho Operations Office

DISCLAIMER

DOE/EE -- 97000108

Assessment Of Strength-Limiting Flaws In Ceramic Heat Exchanger Components INEL Support: Fracture Mechanics And Nondestructive Evaluation Technology - Final Report

W. R. Lloyd
W. G. Reuter

Published June 1993

Idaho National Engineering Laboratory
Metals and Ceramics
EG&G Idaho, Inc.
Idaho Falls, ID 83415

Prepared for the
U.S. Department of Energy
Office of Industrial Technologies
Under DOE Idaho Operations Office
Contract DE-AC07-76ID01570

ASSESSMENT OF STRENGTH-LIMITING FLAWS IN CERAMIC HEAT EXCHANGER COMPONENTS

INEL SUPPORT TASK: FRACTURE MECHANICS AND NONDESTRUCTIVE EVALUATION TECHNOLOGY

ABSTRACT

An examination of a siliconized SiC material, CS101K, has been performed to determine if linear fracture mechanics concepts can be used to characterize and predict the behavior of this material. Phase II of this project showed that a value that appeared to represent the true fracture toughness could be measured using small specimens with a machined notch, if the notch root radius was less than 75 μm. Methods to produce sharply cracked specimens were then investigated to verify this hypothesis. A new technique, called the "beam support" precracking method, was subsequently developed and used to make sharply cracked SE(B) specimens. Tests of these specimens showed a slightly rising R-curve-type of behavior, with elevated values of plane strain fracture toughness. Interference of the crack surfaces in the precrack wake was hypothesized as the most likely cause of these phenomena. Subsequent testing with various precrack lengths provided preliminary verification of the hypothesis. Test results show that, for fracture mechanics-based design and assessment, adequate values of fracture toughness can be obtained from EDM-notched specimens, instead of the more costly precracked specimens. These results imply that, for the Si-SiC material tested, caution is warranted when using any of the methods of assessing fracture toughness that use a sharp precrack. It is also reasoned that these results may generally be more applicable to the coarser-grained structural ceramics that exhibit a rougher fracture surface.

Based on results of testing EDM-notched bend specimens in 1250°C air, no degradation of material properties were observed for exposures, under applied stress, up to 900 h. Instead, some increase in fracture toughness was measured for these conditions. These same tests indicated that the threshold stress intensity factor for stress corrosion cracking (static fatigue) in the hot air environment was the same as the fracture toughness. Assessment of these mechanisms was hindered because the proposed high temperature moiré interferometry system could not be developed to a working prototype. It is still uncertain whether sharp, tightly closed cracks may behave differently, due to uncertainties of the precise mechanism of environmentally-assisted cracking (if it does occur). However, it was determined that localized creep behavior in the notched bend specimens was most likely responsible for the observed increases in fracture toughness.

EXECUTIVE SUMMARY

In 1985 the Department of Energy's Energy Conservation Program initiated a project with Babcock and Wilcox (B&W) to perform proof-of-concept tests of a full scale, high temperature, burner duct heat recuperator. The primary components of the heat exchanger were specified to be siliconized SiC ceramic materials. Methods to assess suitability for service of the structural components (quality assurance) and to estimate performance lifetime were required. The INEL work was performed in three phases beginning in 1985 and continuing through 1992. Both NDE and assessment methodology requirements were addressed in three phases. In Phase I, a lifetime prediction methodology for this class of material was developed. Phase II work developed baseline fracture property data specific to the CS101K material to support the assessment methodology. Specialized ultrasonic transducers were developed and optimized, and tube scanning systems were built for the quality assurance task. The test results and literature studies in the Phase II work revealed two areas of concern. First, What effect does the test specimen notch/crack geometry have on the measured fracture toughness? Second, What effect does the operating environment have on the material's fracture toughness over time (property degradation)? The Phase III work addressed these two issues; both are important in achieving reliable results from the linear fracture mechanics-based assessment and prediction methodology.

Based on the results of fracture toughness tests using both EDM-notched and sharply precracked test specimens, the fracture toughness values measured using the EDM-notched SE(B), A(B), or externally notched C-ring compression specimens are adequate for design purposes. Saw-cut notches possibly could be used in place of the EDM notches. To make this determination, a new method for introducing sharp-tipped precracks in brittle ceramic materials, the "beam support" technique, was developed and successfully applied.

Results of the sharp precrack toughness tests showed a variation in measured toughness with precrack length. This led to the hypothesis that crack wake interference was affecting the toughness measurements. Subsequent tests showed a correlation between length of precrack (crack area) and measured fracture toughness. An apparent rising crack growth resistance was noted during fracture toughness testing using the sharply precracked SE(B) specimens.

The test results from elevated temperature testing in air indicate little effect of environment on fracture behavior, i.e. cracking processes, of the CS101K siliconized SiC material. Time at temperature and stress do not appear to effect actual crack growth resistance in this material at the temperatures and stress (stress intensity) levels investigated, although an apparent elevation in the material's fracture toughness was observed after the combined temperature/stress exposure. It is believed that a localized creep phenomenon may be responsible.

A total methodology for making conservative (safe) predictions of critical flaw sizes in Si-SiC ceramic tube components was successfully developed, including a modest sized database of supporting material property information. The predictions are accomplished by using measured fracture toughness values, suitable stress intensity factor calibration equations, and realistic estimates of the applied stresses (or design allowable stress) the component will experience. The conservatism of the predictions made using this methodology are increased for crack-like defects, based on the results of the sharp crack tests made in Phase III. This is based on the observations that the EDM-notched specimens provide a minimum value of fracture toughness, and that "real" cracks (sharp-tipped with rough, interacting faces) show an effectively higher toughness with increasing crack growth resistance as the crack extends.

The test results obtained in this work indicate that the fracture toughness values obtained from room temperature tests of mechanically notched (by EDM or diamond machining) specimens can be used to provided a conservative estimate of servicability over the range of temperatures expected in operation. Special preparation of test specimens to provide sharp-tipped precracks is not required, as this appears to artificially elevate the measured fracture toughness. Testing at elevated temperatures is not required, since no degradation of fracture toughness was observed. Using room temperature values will serve to provide a small amount of conservatism in the results of the analysis.

CONTENTS

LIST OF FIGURES

LIST OF TABLES

GLOSSARY

COD gage - Crack opening displacement gage. A measurement device commonly used in fracture toughness testing. The standard design uses electric strain gages mounted to parallel cantilever spring beams. The free tips of the beams are grooved to fit small "knife edges" mounted across the crack mouth to measure the opening displacement as forces are applied.

Natural Crack - Also called a sharp crack or sharp-tipped crack. For the purposes of fracture testing, it is usually a planar or nominally two-dimensional defect in a test specimen. In most cases it has been introduced into the specimen in a controlled process, to simulate a "naturally" occurring defect (one that is generated through materials processing, manufacturing, or in-service conditions). The radius of the crack tip must be very small to be considered a natural crack.

Pop-In - A crack growth (extension) event, typified by high growth rate, but where the crack front stops advancing prior to complete separation of the specimen or structure into two pieces.

Precracking - Any procedure where a natural crack is introduced into a test specimen in a controlled manner, in a preselected location and at a prescribed orientation, to a predetermined size. Precracking is done to prepare test specimens for fracture toughness testing.

Sharp Crack - see Natural Crack.

ASSESSMENT OF STRENGTH-LIMITING FLAWS IN CERAMIC HEAT EXCHANGER COMPONENTS

INEL SUPPORT TASK: FRACTURE MECHANICS AND NONDESTRUCTIVE EVALUATION TECHNOLOGY

1. INTRODUCTION

In 1985 the Department of Energy's Energy Conservation Program initiated a project with Babcock and Wilcox (B&W) to perform proof-of-concept tests of a full scale, high temperature, burner duct heat recuperator. The system was designed to recover waste heat from a steel soaking pit and reuse the energy to preheat the combustion air to temperatures of about 980 to 1000°C. This was done by using the high temperature properties of silicon carbide (SiC) ceramic materials for the heat exchanger tubes in the system. The heat exchanger system uses a bayonet-type configuration. The inner tubes were a recrystallized SiC (Norton Corporation designation CS101, trade name Crystar) with about 15% porosity and a thin, glazed surface for oxidation protection. The outer tubes were siliconized SiC (Si-SiC); either HD430 with an organic carbon char and about 8% Si metal, or CS101K (siliconized Crystar) that was siliconized by a proprietary process with about 15% Si metal filling the original porosity and virtually no porosity in the final product. The ceramic tubes were expected to be the most critical component in the system, as their failure would seriously jeopardize successful completion of the proof-of-concept tests.

As part of this project, it was necessary to identify performance-limiting conditions in the structure. Methods to assess suitability for service and to estimate performance lifetime were also needed. These requirements necessitated the development of means to identify and to assess strength-limiting defects in the structural components. Nondestructive evaluation (NDE) techniques would be required to detect the defects and an assessment methodology would be required for serviceability and lifetime prediction. The program's technical monitor commissioned work at the Idaho National Engineering Laboratory (INEL) to augment work being performed by B&W.

The INEL work was performed in three phases beginning in 1985 and continuing through 1992. Both NDE and assessment methodology requirements were addressed. In Phase I, a lifetime prediction methodology for this class of material was developed. The methodology was based on linear fracture mechanics modeling. Supporting NDE methods were also developed in Phase I to provide a means of quality assurance for the materials to be used in heat exchanger construction. Phase II work developed baseline fracture property data specific to the CS101K material to support the assessment methodology. Specialized ultrasonic transducers were developed and optimized, and tube scanning systems were built for the quality assurance task. The results of Phase I and Phase II are summarized in the Background Section.

The test results and literature studies in the Phase II work revealed two areas of concern. First, What effect does the test specimen notch/crack geometry have on the measured fracture toughness? Second, What effect does the operating environment have on the material's fracture toughness over time (property degradation)? The Phase III work addresses these two issues; both are important in

achieving reliable results from the linear fracture mechanics-based assessment and prediction methodology.

2. BACKGROUND

2.1 Phase I: Investigation of Lifetime Prediction Methodologies

Phase I (Reuter, 1986) provided an investigation of available methodologies and techniques that could be applied to making lifetime predictions of the tubes. The work also identified the associated requirements for characterizing the tubes[a] so that the lifetime predictions could be made. A lifetime prediction model based on linear elastic fracture mechanics (LEFM) was proposed that would give a conservative estimate of minimum lifetime for the ceramic tubes. That model was used with the limited fracture toughness (K_{Ic}) data that existed at the time and operating conditions supplied by B&W to provide some preliminary lifetime estimates of the tubes. Recommendations were also made for further research that should improve the accuracy and reduce the conservatism of the estimates. They included various aspects of mechanical and environmental effects on cracking of the SiC materials. In order of importance, they were: (1) Effects of the environment on fracture toughness and crack growth, (2) improved estimates of the stresses and stress gradients in the tubes, (3) accurate knowledge of sizes and distributions of defects in the new tubes, and (4) a better database of fracture toughness at various temperatures for the SiC material. During the Phase I work at INEL, B&W developed and applied NDE techniques to examine the ceramic tubes for defects. The techniques of microfocus radiography, scanning laser acoustic microscopy (SLAM), pulse-echo acoustic microscopy (developed at INEL, also called time-of-flight acoustic microscopy, or TOFAM), and acoustic backscatter mapping were identified as the four techniques with the best chance of providing the required information on defect sizes, orientation, and location.

2.2 Phase II: Development of Supporting Data

Phase II work at INEL primarily focused on solutions to items (1), (3), and (4) mentioned above. This included the development of improved NDE capabilities to provide the required defect detection capabilities for (3) and investigating the fracture mechanics details of (1) and (4). Kunerth and Johnson (1987) worked on optimizing the ultrasonic transducer design for scanning the tubular shapes with the TOFAM system. They developed a method to optimize the ultrasonic transducers for particular shapes to be scanned (in this case, tubular). Three primary scenarios of failure were identified, and all were fracture-related. The first was the existence of a large defect, undetected during preservice inspection (failure of NDE technology), that initiated a catastrophic failure during initial start-up or during an allowable transient peak in stress during operation. The second mechanism was subcritical crack growth (mechanically and/or environmentally assisted), where a small crack grows to critical size, and initiates a catastrophic failure under normal operating conditions. The third area of concern was a degradation of the material's properties through exposure to the operating environment, primarily a reduction in fracture toughness, which would lead to a catastrophic failure of the structure under supposedly safe design conditions.

Improvements in NDE technology addresses the first of the three failure scenarios, where structural failure is caused by an NDE/preservice inspection quality control failure. However, the probability of detecting all defects of concern will still be less than 1.0, so it will be necessary to either accept some premature failures or devise a proof testing program to augment the NDE inspections. The other two scenarios require further knowledge of environmental effects on the material and its fracture behavior. Although the environmental effects to be determined were identified, a method to measure them had to be developed. Additional knowledge of the specific

fracture behavior of the material (independent of environmental effects) also had to be developed. Some of these fracture behavior and environmental effects issues were resolved through an extensive test program performed during Phase II.

The test program investigated various specimen configurations that could be used to measure the material's fracture toughness, including single edge notch bend [SE(B)], arc-shaped bend [A(B)], and notched C-ring compression-type specimens. The Norton CS101K Si-SiC was used throughout all of this testing. All three specimen geometries were determined to be satisfactory for fracture toughness testing of tubular-shaped ceramics. For absolute accuracy of test results, the SE(B) specimen was preferred because the standard deviation of the test data was smaller than for the other geometries. The notched C-ring compression specimen is preferred for ease of fabrication and simpler set-up for elevated temperature testing. The A(B) specimen is beneficial because it requires the least amount of material to make individual specimens.

The effect of the machined notch root radius on measured fracture toughness was also determined. As expected, a larger notch root radius increased the measured value of critical stress intensity, K_Q.[a] Based on results of these tests of specimens with width (W) of 5 and 10 mm and various notch root radii, a machined notch with a root radius less than 75 μm will yield a critical stress intensity value that can be accepted as the fracture toughness, K_{Ic}. Fracture toughness variability of the material was also investigated by testing a number of specimens from three different tube segments. K_{Ic} did not vary significantly for the lot of material represented by the tube segments that were tested.

Surface-cracked bend [SC(B)] specimens (which more closely simulate a cracked structural component) were also tested to help verify the fracture mechanics-based design and assessment approach. SC(B) specimens with a range of semielliptical surface notch sizes (made by EDM machining) were tested. The smallest notches were approximately eight times the area of the largest observed porosity (about 90 μm) in the material. The largest notches corresponded to the approximate size of a critical defect, based on the fracture mechanics-based design and B&W-specified operating conditions. Test results showed that fracture mechanics-based design methodology could be used to specify allowable initial defect sizes without being overly conservative.

To provide additional verification of the proposed fracture mechanics-based model, a fixture was built to load tubular segments by internal pressurization at room temperature. Four tube specimens, with various size semielliptical or part-circular artificial defects placed axially on the outer surface by EDM, were then tested. The results of the tests were varied, and failed to provide a strong verification of the methodology when predictions were based on the fracture toughness measured using the SE(B) specimens. These tube segments were supposed to be from the same lot of material tested earlier in Phase II, but thickness variations and different interior surface appearance suggested otherwise. No material from the pressure-tested segments were available for fracture toughness testing to verify it, but it is possible that KIc may have been different for those tube segments.

SE(B) specimens were tested in a 1250°C air environment to measure the change in fracture toughness due to increased operating temperature. Standard fracture toughness tests (monotonically

---

a. The characterization of the tubes was to rely heavily on nondestructive evaluation (NDE) to detect cracks and related defects, but some proof-testing to provide verification was indicated.

increasing loading over a short time period) showed KIc to increase from nominally 3.0 MPa$\sqrt{m}$ at 20°C to 3.8 MPa$\sqrt{m}$ at 1250°C, without consideration of other environmental or time-dependent effects.

Some long term, constant load tests were also conducted in air at 1250°C to begin an assessment of elevated temperature environmental effects. Of specific interest was crack growth by the so called "static fatigue" mechanism. Tests were performed using the SE(B) specimens in a constant load fixture at elevated temperature. They were conducted with loads that produced varying levels of applied stress intensity up to and in excess of the monotonic fracture toughness. One test, at an applied K of 3.7 MPa$\sqrt{m}$ (95% of the mean fracture toughness) at 1250°C, survived in excess of 900 h. No macroscopic creep, manifested as permanent deformation of the specimen, was observed for this specimen. The results of these tests pointed to the probability that static fatigue mechanisms would not lead to a catastrophic failure of a component. An apparent toughening phenomenon was also observed for notched specimens that were held at 1250°C with a (unspecified) load applied. This toughening was more pronounced at 1250°C (three specimens) than at room temperature (two specimens) based on results of five tests. The tests at 1250°C resulted in apparent toughness values of 4.90, 5.84, and 6.34 MPa$\sqrt{m}$, while the room temperature tests gave values of 3.7 and 3.8 MPa$\sqrt{m}$.

Examination of the results of the long term elevated temperature tests suggested that the threshold stress intensity for static fatigue (K_{th}) was not measurably lower than K_{Ic}, based on data for up to 900 h of exposure. However, caution was advised in extrapolating this value to longer times since the mechanism(s) that could be operating were unknown.

2.3 Phase III: Effects of Sharp Cracks and Environment

A list of suggestions for continued research areas was also provided at the conclusion of the Phase II report. There were three main topics in the list. Observations that showed the static fatigue threshold to be about the same as the fracture toughness, and that showed increasing toughness after being stressed at 1250°C, suggested that further assessment of mechanisms of environmentally-assisted crack growth was in order. A need to verify the values of K_{Ic} and K_{th}, as well as determining crack velocity data, using naturally-cracked specimens instead of EDM-notched specimens was identified. Further verification of the proposed fracture mechanics-based methodology was also indicated, by additional testing using the tubular specimens with various types of defects in them. Advancements in certain technologies were identified that would be required to accomplish the first two of these three goals. Development of a high temperature, high resolution displacement measurement system would improve the chances of precisely isolating the mechanisms that produce the observed material behavior identified above. A method to introduce repeatable sharp-tipped cracks of controllable size in the ceramic materials would also be required.

Based on these recommendations, a work plan for Phase III was developed. Development of the required technologies was the primary focus of the Phase III work, since without them, the remaining goals could not be accomplished. Of foremost importance (first priority) was developing a method to introduce sharp-tipped cracks with relatively large size and controlled shape into the ceramic materials. This would allow test specimens to be made that would precisely simulate the behavior of a real crack in a ceramic structure. Concurrent with this work, the development of a high temperature moiré interferometry (HTMI) system was pursued (second priority). If successfully developed, such a measurement system would allow high resolution displacement data to be collected in the vicinity of the tip of a crack in a test specimen subjected to elevated temperatures. It was

believed that such measurements would lead to further knowledge of cracking mechanisms in elevated temperature conditions.

3. MATERIAL AND SPECIMEN PREPARATION

The material used in this study was the Si-SiC material produced by Norton Corporation with designation CS101K (siliconized Crystar). The material's nominal properties are given in Table 1. The bulk material received from Babcock and Wilcox Lynchburg Research Center (B&W-LRC) for our test program was in tubular form, with nominal 75 mm outside diameter and 6.5 mm wall thickness. The tube forms are produced in 2 to 2.5 m lengths with one closed end by slip casting a SiC slurry, followed by drying and sintering. The resulting material has a bi-modal grain size distribution of nominally 5 and 50 mm with about 15% porosity. A Norton proprietary process is then used to infuse metallic silicon into the pore space in the material. The resulting material has almost no porosity on the grain size scale. Occasional large empty pores up to about 1 mm were observed. A micrograph of the material's structure is shown in Figure 1.

Figure 1. Norton CS101K Si-SiC

Table 1. Properties of CS101K

Chemical Analysis (Volume Percent)	85% SiC, 14% Si metal, 1% Impurities
Density	3.0 gm/cc
Apparent Porosity	0%
Modulus of Rupture	255 MPa @ R.T, 172 MPa @ 1250°C.
Modulus of Elasticity	276 GPa
Thermal Conductivity	54 W/mK @ 1200°C
Coefficient of Thermal Expansion	4.8×10^{-6}/°C
Maximum Use Temperature (suggested)	1350°C

Information in this table is from the Norton Advanced Ceramics Technical Bulletin for "siliconized Crystar" dated October 1990.

The pieces of tube received at INEL from B&W had been cut to 300 mm lengths and were not identified as to their relative position along the length of the original tube. Most of these segments had an identifying number written on them. The significance of these markings could not be determined, but they probably identified which whole tube the segment was removed from. The outer diameter of the tubular pieces were relatively constant, but substantial variation between 5.5 and 7.0 mm in wall thickness was noted. The SE(B) specimens were made from the thicker-walled tube sections. The character (roughness, asperities, etc.) of the inside surface of the tubes varied considerably, too. After discussing these variabilities with B&W-LRC, we felt that all of these variabilities could be attributed to the slip casting manufacturing technique used in the production of the tube forms. INEL apparently received a random selection of material from the entire lot ordered by B&W. Because of this, the thickness variations could not be assessed any further. The wall thickness variation is probably due to slumping of the slurry towards the bottom end during drying (assuming the slips are dried in a vertical direction). No direct information on quality control and dimensional variability could be obtained from Norton, but contacts at B&W-LRC suggested that the variation observed in the pieces received at INEL are typical and would be representative of the actual

components used to build the type of heat exchanger described in the first part of the Background section.

In Phase II of this support work performed at INEL (see Reuter et al., 1989), several different types of standardized (for metals) fracture toughness test specimens (see the Annexes to ASTM E 399-90, 1991) were used to assess possible anisotropic fracture toughness of this slip cast Si-SiC material. Since the toughness of the material was found to be independent of the crack plane orientation and crack growth direction, all work in Phase III was carried out using a small scale, single edge notch bend [SE(B)] specimen. The SE(B) specimen geometry is well characterized, is relatively easy to fabricate by grinding operations, and most importantly, is the one specimen design that is amenable to the sharp crack precracking procedures.

3.1 Generating Sharp-Tipped Cracks (Precracking)

A principal goal of the Phase III work was to assess possible differences in fracture toughness and related phenomenon that could be attributable to the geometry of the crack tip. In the prior work of Phase I and Phase II, the EDM process was used to insert defects (notches) of controlled geometry (shape and size) into the Si-SiC ceramic material. This is discussed in detail in the report of the INEL support work for Phase II (Reuter et al., 1989). The crack tip geometry produced by wire-type EDM is typically of fairly uniform radius. This radius was minimized to the extent possible at the time as limited by the EDM process. Although a radius of 60-70 μm could be regularly achieved, which is relatively small compared to the notch length and specimen dimensions, it is large compared to a naturally occurring crack tip (sub-micron) and the smaller microstructural dimensions (e.g. grain boundary length, grain size, and voids). The EDM notches also prevented assessment of any wake effects that could occur in a natural crack, which has inherent roughness on the crack faces that could interact to effect the measured fracture toughness of the material. A method to assess these effects would be required, where sharp, natural cracks could be generated in a precise, controllable manner.

3.1.1 Precracking Using the "Bridge-Indentation" Method

The bridge-indentation precracking method (Nose and Fujii, 1988) involves two basic steps. First, a pyramidal diamond indentor (standard Knoop-type hardness indentor) is used to place a starter defect on one surface of the rectangular bar specimen. This specimen is then placed in the support bridge base with the starter defect centered between the pedastles. A solid pressing bar is placed on top of the specimen (side opposite the starter defect). A schematic diagram of the bridge fixture is shown in Figure 2.

The specimen is then loaded by applying increasing force to the pressing bar until the desired precrack "pops in" (see Glossary) from the starter defect. The size of the resulting precrack is dependent on bridge fixture geometry and starter defect size (and likely the materials fracture properties). The starter defect size is controlled to some extent by the maximum indentor force used. Professor Bar-On at the Worcester Institute suggested trying the bridge-indentation method which she had used with good success in some of her research work (Bar-On, 1990). The work presented by Fujii and Nose (1989) indicated the method's ability to produce

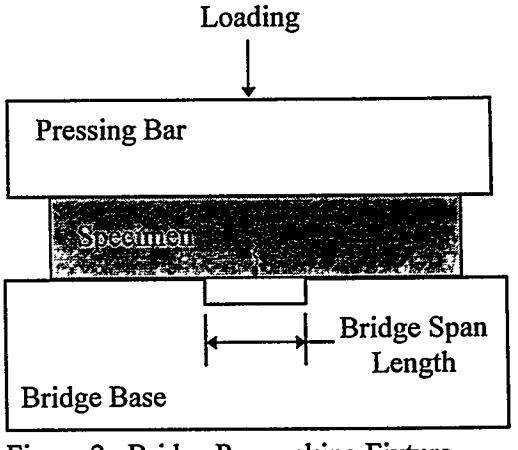

Figure 2. Bridge Precracking Fixture

relatively long cracks in a reproducible manner in various fine-grained ceramics.

Eight prepared rectangular bars (plain bars, ground to size, without notches) were sent to Prof. Bar-On at Worcester Institute to precrack using the bridge-indentation method. (They had the required fixtures and had some prior experience in applying the method). The initial results obtained from the work at Worcester Institute were not particularly encouraging for several reasons. The overall precrack lengths (a_{avg}, see Figure 3) varied considerably, presumably due to differences in the starter indent force, which has to be varied to give the desired precrack length. Apparently, this force is quite material dependent, and the relationship of indent force to final precrack length must be empirically determined. There was also an undesirable amount of in-plane crack front curvature (unevenness in length) in several of the specimens. No direct explanation for this variation in curvature can be given, but it may be due to slight misalignment of the starter indent or other factor associated with the production of the starter indent. Out-of-plane crack front curvature was typically small and acceptable for the purposes of the proposed testing.

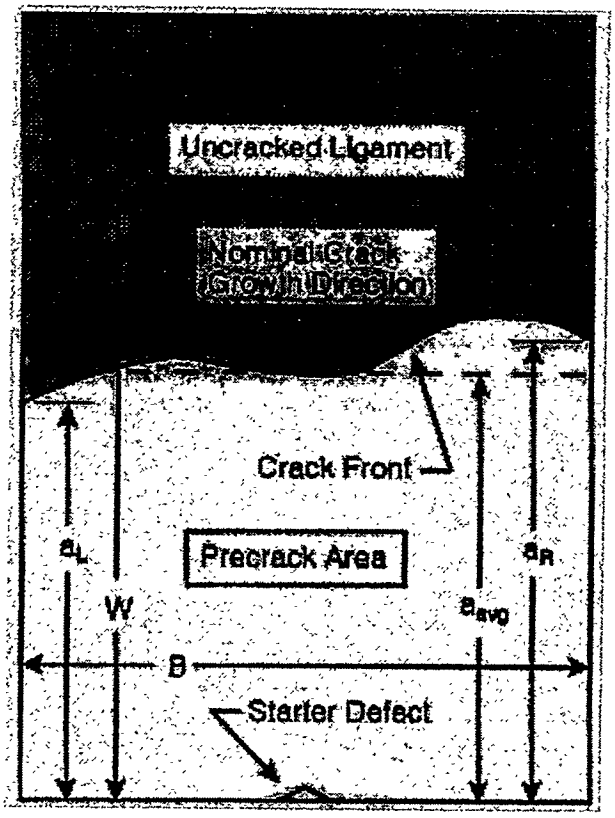

Figure 3. Sharp precrack geometry.

For comparison and verification, three of the eight precracked specimens were tested at Worcester Institute, and the remainder were returned to INEL for testing. The three Worcester Institute test results were questionable due to some of the difficulties associated with fracture toughness testing. In this case, it is difficult to determine what the maximum applied load (failure load) will be prior to the initial test. The maximum load on the recorder was exceeded prior to specimen failure in one instance. The exact load scale calibration was in question on the other two, so the critical load values cannot be determined for these tests with high certainty. Attempts to clarify the data and recover meaningful results were unsuccessful because students who had worked on the specimens and testing had left the department and were the only possible source for reconciling the data. The remaining five precracked specimens were returned to INEL, along with their precracking data (indent force, precrack pop-in load, etc.). These parameters are given in Table 2.

It was hoped that better control of the precracking process, and more accurate determination of the correct indent load for the desired crack length, would yield acceptable precracked specimens using the bridge-indentation method. INEL used the Worcester Institute-supplied precracking data to the extent possible, and attempted precracking of additional specimens using the "bridge-indentation" method. Various starter indent loads from 50 to 500 N (maximum force allowed for the Vickers pyramidal diamond indentor by the equipment owner), bridge spans from 5 to 20 mm, and pedastle widths from 10 mm to full specimen length were tried. However, uniform crack lengths were almost unobtainable and the variability in precrack "pop-in" load from one specimen to the next was large. On some specimens, the expected pop-in load was exceeded by a factor of 5 and no pop-in occurred.

The attempted precracking at INEL used acoustic emission to detect the precrack pop-in event. It is not known how pop-in was detected for the specimens prepared at Worcester Institute, although it is believed that AE was used.

Table 2. Results of initial precracking effort.

Specimen ID[a]	Indentor Force (N)	Precrack Pop-In Force (kN)	Bridge Span (mm)	Crack Length[b] (mm)	Dimensions[c] (mm)		Comments
					W	B	
2I-1*							
2I-2	294	22.24	5.0	6.0	7.96	5.18	
2I-3	343	10.00	6.0	3.7	7.99	5.16	
2I-4	343	9.79	6.0	2.4	7.97	5.20	
2I-5*							
2I-6*							
2I-7	343	9.79	6.0	4.3/2.0	7.97	5.18	crooked crack
2I-8	343	11.12	6.0	3.8	7.97	5.19	

a. "*" designates specimens tested at Worcester Institute.

b. Average lengths as measured on opposite sides of the specimen at Worcester Institute.

c. Dimensions W and B. W is parallel to the crack growth direction; B is approximately parallel to the crack front and normal to W.

Observation (SEM and optical microscope at 800x) of the specimens that were precracked with the "bridge-indentation" method also revealed some secondary cracking of the specimens near where the inner edges of the two pedastle portions of the fixture base contacted the specimens.[a] Figure 4 shows the relationship of bridge indentation fixture base, applied loading, specimen, and observed cracks. There was a dimension of the precracking bridge support fixture, the width of the two "pedastles," that was not directly identified by either Nose and Fujii or by Worcester Institute. The Nose and Fujii paper (1988) only mentions that the pedastles did not extend past the end of the specimen length. The attempts at precracking using this method at INEL suggested that this may be a critical dimension required to use the method effectively. It is obvious that this dimension will effect the local stress state around the starter defect, and possibly more importantly, the relative stress state in the specimen away from the starter defect. This could explain some of the secondary cracking that was observed.

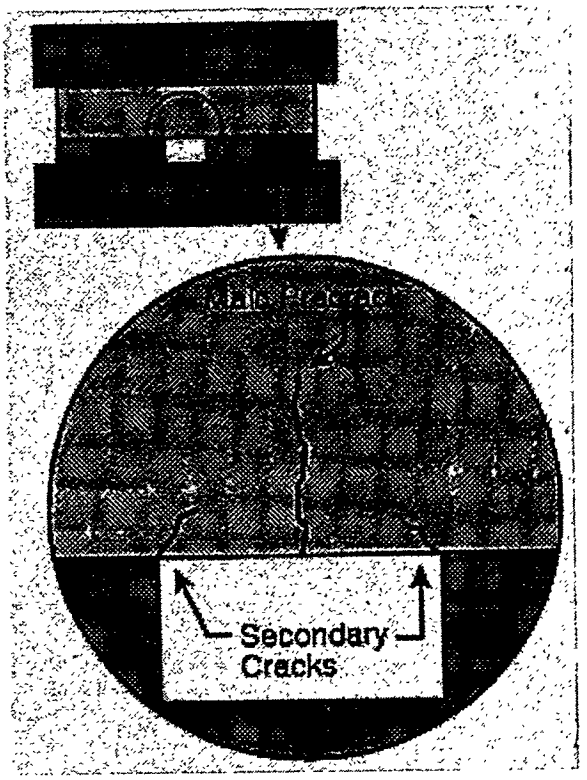

Figure 4. Secondary cracking observed at pedestal corners in SiC specimens.

a. Based on conditions specified in ASTM E 399-90 (1991) being met, K_Q can be accepted as the actual plane strain fracture toughness, K_{Ic}.

After several weeks of working with this technique, it was abandoned because of time constraints and lack of success in routinely producing acceptable precracks. While there was evidence that it would work for uniform, single phase, fine-grained ceramics (e.g. alumina, as presented in Nose and Fujii, 1988; Fujii and Nose, 1989; and Bar-On, 1990), the results obtained at INEL suggest that the technique does not work well to precrack the coarser-grained, multi-phase Si-SiC (nominally 5 and 50 μm SiC grains forming a continuous matrix with Si metal filling most of the intergranular space) used in the present study.

Some details of local stress intensity distributions around the starter indent were given in Nose and Fujii (1988). Further investigation of the stress fields around the indent and at the pedastle edges for various indent loads, bridge spans, and pedastle widths may lead to additional understanding of these problems. However, these details were not investigated since the procedure was being abandoned due to constraints mentioned above.

3.1.2 Development of the "Beam Support" Method for Precracking

Following the failure of the bridge-indentation method to produce acceptable precracks, an alternate approach was developed at INEL. This is called the "beam support" method for precracking based on the geometry of the fixture. The set-up is shown in Figure 5. The method was based on the idea of minimizing the strain energy release rate in the specimen "system." While the bridge-indentation method accomplishes this to some degree, it primarily operates by providing a compressive stress field ahead of the crack which is somewhat independent of the crack length. The dynamically extending crack (pop-in crack) is arrested as it grows into the compressive stress field. The beam support method allows for stable crack extension by controlling the energy that is released during a small increment of crack extension. The beam support method does this by providing an effective stiffening of the specimen and loading apparatus, such that the strain energy release is very localized around the crack tip. The cracked specimen cannot freely deform (with respect to load line displacement) when the crack advances, due to the uniform (in a gross sense) supporting force of the solid beam under the notched specimen. The effect is that of having a large stress decrease around the crack tip for a small amount of crack extension.

The local crack tip stresses and strain energy release rate is probably similar to that of a very deeply cracked bend specimen, which is known to have higher crack growth stability than similar specimens with shorter cracks (see Baratta, 1988). This observation is based on the observed stable crack growth behavior using the beam support configuration. A crack growth stability analysis was not attempted for the beam support configuration since it was found to work by experiment. Such an analysis would likely be quite difficult due to the indeterminant nature of the geometry.

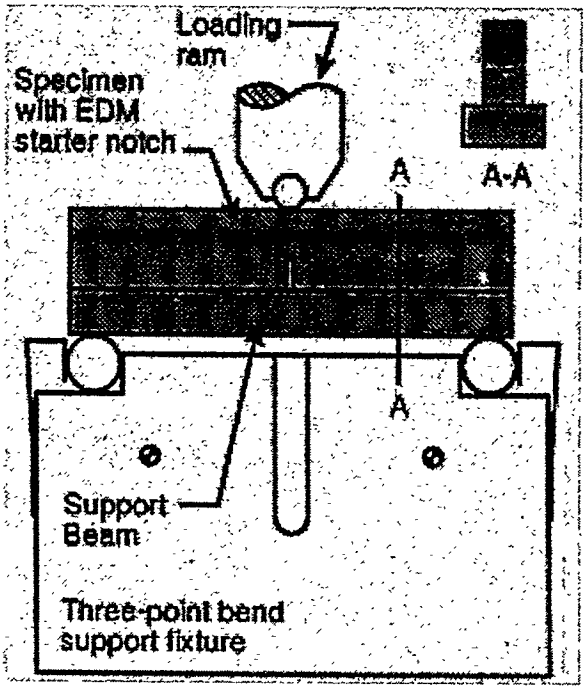

Figure 5: Setup for beam support precracking method.

Effects of the specific geometry of the beam support set-up were not examined either. The standard three-point bend fixture with a 40 mm span was used. The support beam was just a regular, unnotched specimen blank (5 x 10 mm) laid on its side across the support rollers. A thin layer of silicone-based ultrasonic couplant gel was placed between the support beam and the specimen to transmit the acoustic emission waves (created at precrack pop-in) from the specimen to the support beam where the AE transducer was mounted. The couplant gel probably reduced friction between the specimen and support beam. Regardless of these unknowns, sharp cracks were successfully extended in a controlled fashion from the tips of EDM crack starter notches in the Si-SiC specimens using this beam support method.

4. CRACK LENGTH ASSESSMENT

The crack lengths in the specimens used for fracture toughness testing must be accurately measured for the testing results to be accurately assessed and converted into fracture toughness data. For test results to be valid, certain crack geometry criteria must be met, including average length, length variation, crack front curvature, and crack plane curvature. Careful monitoring of crack length during precracking is important to maintain a valid crack geometry. This is a straightforward task with most metallic specimens that are precracked by high cycle fatiguing. Crack growth is slow and controlled, and the position of the crack is easily monitored at the specimen surface under moderate magnification (usually 5 to 20x) during the fatiguing process. After a specimen is tested (specimen is broken in half and crack surfaces are exposed) the interior geometry of the crack must be examined to ensure validity of the test results. Again, this is a routine procedure for metallic specimens. The boundary between the precrack and the final fracture is delineated by an easily recognizable change in the surface roughness. Therefore, the geometry of the precrack can be readily measured. This is not the case, however, for the Si-SiC ceramic specimens used in this work.

Precracking the Si-SiC specimens using the bridge-indentation method described earlier is essentially a one-shot proposition. The specimen is prepared and then loaded until crack pop-in occurs. The length of the precrack produced is then measured. If it is acceptable, the specimen is ready for testing. If it is too long or short, the specimen is generally ruined and is discarded.[a] This is not usually the case for specimens prepared using the beam support precracking method. The beam support method starts with a relatively large starter notch, from which a sharp precrack is slowly extended in a stable manner. To produce an acceptable specimen, this crack extension has to be monitored to determine when an acceptable crack length is reached. The following discussion explains some of the difficulties encountered and some partial solutions that were developed for measuring precrack lengths.

4.1 Measuring Precrack Lengths

The precrack extension could not be visually monitored in real time due to the high magnifications required to see the crack. This resulted in a multi-step procedure being required to precrack a specimen. It involved loading a specimen into the beam support precracking fixture, applying some increment of additional load (higher than the previous maximum) to induce an (unknown) increment of crack extension, unloading the specimen and removing it from the fixture, and then optically examining the surfaces to see how much, if any, detectable crack extension had occurred. This process was repeated until a precrack of desired length was obtained. As can be imagined, this is a laborious and time-consuming procedure.

4.1.1 Optical Measurements

Measuring the precrack lengths on the specimen surface of this Si-SiC material is quite difficult. The elastic modulus of the material is about 30% higher than steel and the toughness is very low compared to brittle metals. Even with some load applied to open the crack (which must necessarily be small to prevent breaking the specimen), the crack opening displacements are very small and cannot be reliably seen below about 200-400x magnification. No equipment was available

a. There are procedures, such as reversed bending fatigue, that can be employed to lengthen a crack that is too short or to straighten a crack that has too much length difference through the specimen thickness. Specimens with cracks that end up too long for standard tests may sometimes be used for special tests.

to examine the specimens under load at these magnifications, so specimens had to be removed from the precracking fixture and taken to an optical microscope for examination.

The Si-SiC material is completely elastic at room temperature, so there is no residual plasticity around the precrack tip or the crack wake to provide a residual crack opening. The crack opening that does occur during precrack extension is very small due to the low toughness of the material. (Crack opening, d, is proportional to applied load, which is dependent on fracture toughness, for crack extension to occur.) Because of this, there is little chance for asperities or debris (such as dislodged grains) in the crack wake to move so that the precrack is held slightly open when the precracking load is removed. These factors make the crack difficult to see because it is closed so tightly. The surfaces of the specimens must be highly polished (1 mm diamond film polishing was found to be adequate) prior to precracking to make the tightly closed cracks visible. The nature of the polished surfaces (bi-modal grain size distribution, 5 and 50 μm, with the interspersed Si metal) creates a large contrast variation in the magnified image between the Si metal and the SiC grains. Contrast variation between the crack line and the material is all that distinguishes it, since there is no detectable surface relief associated with the crack (as there would be with an open crack). In fact, as the crack tip region is approached, the crack is closed so tightly that localized diffraction-induced interference seems to be all that makes the location of the crack apparent. At this point, the crack is no longer visible as it crosses SiC grains; it is only apparent where it crosses the Si metal islands.

It is not usually too difficult to locate the origin of the precrack using 100-200x magnification. For the bridge-indentation precrack, the origin is along the bottom edge of the specimen; it is at the starter notch tip for the beam-support precrack. The initial portion of the crack is tracked along the surface until it can no longer be seen. The magnification is then increased to 600-1000x, and the crack is followed some additional distance until it traverses a Si metal island, and apparently ends at the boundary of the Si metal island and a SiC grain. By visually searching the perimeter of the SiC grain or SiC grain cluster where the crack appears to end, the crack will usually be found to reappear crossing an adjacent Si metal island. This search can be repeated until the apparent terminus of the crack is found. During this final search procedure, manipulation of the light controls and the focus must be used to reveal the crack, as explained in the previous paragraph. Because the size of the larger SiC grains do not usually exceed 50 μm, the surface position of the crack tip can be established fairly accurately (within the nominal 50 μm grain size or less) using this technique.

Understandably, repeated visual examinations of the specimen to determine crack extension were very tedious and required an experienced microscopist to detect and reliably measure the crack lengths. Considering that this measurement procedure had to be repeated (typically) ten times for each specimen before an acceptable precrack length was obtained, alternatives were sought to speed up the precracking procedure. The two ideas that were employed were acoustic emission correlation and elastic compliance crack length estimation. The development and use of these techniques proved to assist in the beam support precracking procedure by significantly reducing the number of visual inspections required for each specimen.

4.1.2 Acoustic Emission Correlation to Crack Extension

Acoustic emission (AE) monitoring (see the Appendix on Acoustic Emission) was already being used to detect crack extension. It was originally being used to detect the pop-in event for the bridge-indentation method. Once that technique was abandoned, the AE system was being used to detect the onset of crack extension using the beam support precracking method. The AE system collects and processes data in various ways. It was decided to investigate the possibility of

correlating some measurable AE parameter with the amount of crack extension occurring, to lessen the requirement of the repeated visual measurements of crack length.

By comparing the various AE parameters (events, ringdown counts, amplitude, energy, etc.) obtained during precracking with physical measurements of crack extension, an approximate correlation was found between cumulative AE energya and the amount of new crack surface that was created. The particulars of the correlation are extremely dependent on many parameters of the set-up, including specimen geometry and damping, transducer/specimen coupling, transducer sensitivity, preamplifier gain, amplifier gain, background noise level, trigger threshold level, and processing capabilities of the particular AE system being used. For these tests, the AE system was an AET Model 5500. An AET Model MAC425 transducer was used and was coupled to the support beam with a beeswax couplant. The support beam was, in turn, coupled to the specimen with a silicone-based gel. The MAC425 transducer had a nominal sensitivity of -95 dB relative to 1V/mbar over the frequency range of 150 kHz to 600 kHz with a peak of -82 dB at 450 kHz, per its data sheet. An AET Model 160B preamp with 60 dB gain was used between the transducer and the main amplifier and signal processor. Main system gain was set at approximately 30 dB (40 dB times a linear attenuator set at about 35%). The background noise level was about 0.4 Vp-p and the triggering threshold was set at 0.5 Vrms. Typical events had peak amplitudes greater than 2 Vp-p.

The particular algorithm used to determine "energy" is not given in the equipment manual, and the "energy" values are reported in units of dB. Because of these unknown factors and the relatively poor accuracy in making a quantitative crack length or extension measurement, this information should be used with caution. The only way to apply this method is to do a series of experiments and develop a correlation (if it exists) that will be particular to the experimental equipment, test set-up, and material being cracked. The correlation for the set-up described above was about 18000 energy units per 1 mm2 of new crack surface. However, the range for five specimens tested ran from 6000 to 40000 energy units/mm2. Although not too accurate, an estimate of the amount of crack extension during precracking can be made in real time, without continuously removing the specimen from the test fixture for examination under a microscope. By using the approach, the desired crack length was usually obtained with either one or two visual examinations of, or alternatively, compliance measurements on, the specimen.

4.1.3 Compliance-Based Crack Length Estimation

To further assist in determining the length of the precracks in the specimens without the repeated visual measurements, the elastic compliance technique (E 813-89, Annex A1.5, 1991) for crack length estimation was also used. Although it required the specimen be removed from the beam support precracking set-up, little other inconvenience was produced. The technique can be used with the basic three-point bend fixture used for the beam support precracking, by just removing the solid support beam and placing the precracked specimen directly on the support rollers.

A specimen's compliance is defined as the slope of the specimen displacement versus the applied load. The specimen displacement can be either load-line displacement, or alternatively, its crack mouth opening displacement (COD or CMOD). Using the appropriate relations from ASTM E 813-89 for the type of displacement measurement that was made (load-line displacement in the present case), the specimen's compliance and dimensions can be used to determine the effective length of the crack in the specimen.

Compliance measurements are typically made by fitting a COD gage across the crack mouth on the specimen, from which COD compliance can be determined. Load-line displacement (which can be measured in a variety of ways) can also be measured and values of load-line (LL) compliance can be calculated. A number of factors influence the accuracy of these compliance measurements, but it is accepted that COD compliance yields the most accurate crack length estimations. However, the ceramic specimens are so small that no electromechanical COD gage could be used, so the load-line displacement was measured instead. These measurements were made with either of two types of displacement-measuring transducers; a capacitive transducer that measured the mid-point deflection of the bottom of the specimen adjacent to the crack mouth, or an LVDT mounted to the support fixture near the rollers with the core mounted to the loading ram (see Figure 6, p. 17 for details). On some specimens, both measurements were made simultaneously. The mid-span deflection on the bottom of the specimen and the load-line displacement should be essentially the same on these ceramic specimens, and nominally were. However, the capacitive transducer showed some nonlinearity at the start of loading and whenever the displacement direction changed. While the capacitive transducer's location may have a slight advantage in measurement accuracy, the better linearity and repeatability of the LVDT made it the more desirable choice for displacement measurement. All of the latter specimens tested at room temperature, during precracking and during fracture toughness testing, used the LVDT to measure load-line displacement.

In the elastic regime, the load-line displacement is related to COD for a fixed crack length. This relationship is given in Annex A1 of ASTM E 813-89 (1991). Given suitable accuracy, either measurement can be used for a compliance-based crack length assessment. As described above, the load-line displacement was used to obtain the LL compliance, since a COD measurement was not available for the small specimens.[a]

COD compliance-based crack lengths for larger (typically $W \geq 25$ mm) metal specimens are usually within 10% of the average actual length, with 3 to 5% accuracy more common. The amount of crack front curvature, or tunneling, causes most of the error in metal specimens. Load-line displacement measurements on the ceramic specimens tested in this work ($W = 10$ mm) gave LL compliance-based crack length estimates that were within 20% of the lengths measured on the surface of the specimens, with the error always having the actual crack longer than the estimate. The additional error can be attributed to several factors: crack surface roughness, the small specimen size, roller friction, elastic modulus estimates, and the fact that the displacement measurements were remote load-line measurements instead of true COD measurements. The crack surface roughness is expected to be the major contributor to a decrease in the measured effective specimen compliance, predicting a shorter crack, which is what was observed. The error in measured compliance due to fixture friction and LVDT measurement position was verified by testing a solid rectangular bar of known geometry and elastic modulus, from which the theoretical load-line compliance could be calculated.

The LL compliance-based crack lengths, although not highly accurate, were still useful because the error was found to be fairly consistent at between -5% and -15% of actual crack length based on visual measurements of crack length at the specimen surface. By making these crack length estimates, fewer trips between testing machine (precracking set-up) and metallography laboratory were required to visually check the crack extension, saving considerable time.

---

a. For the actual fracture toughness testing using the basic guidelines found in ASTM E 399-90, absolute displacements are not required; only displacement measurement with acceptable linearity. But, in this work that required crack length estimation, good linearity and displacement measurement accuracy were required.

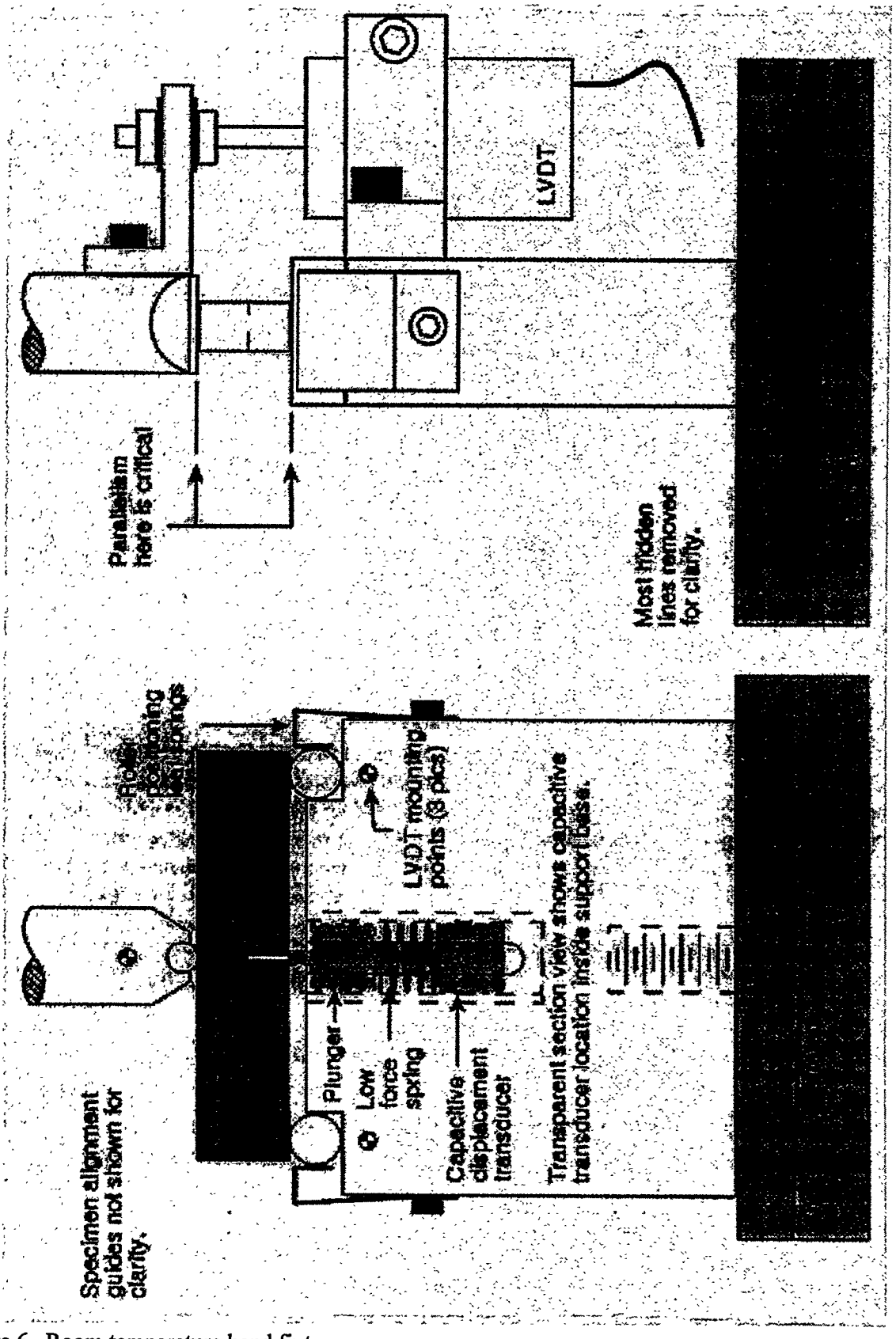

Figure 6. Room temperature bend fixture.

4.2 Post-test Crack Geometry Verifications

Once the actual fracture toughness tests are completed, the crack geometry must be determined to (1) make an accurate calculation of the fracture toughness, and (2) ensure that the test results are valid based on requirements set in ASTM E 399-90 (1991).a An accurate through-the-thickness average crack length must be determined for use in the formula to calculate K_{Ic} using the critical applied load, PQ, determined in the test. For the test results to be considered valid, there are also requirements stated that limit the amount of crack front curvature, overall crack length, and out-of-plane deviation of the precrack surface. The key element in making these determinations is accurately locating the boundary on the fracture surface that separates the precrack area and the final fracture area.

In a typical metal specimen, precracked by high cycle fatigue, the precrack surface always has lower roughness and generally has a flatter topography than the final fracture surface. These differences make the identification of the boundary line between the two areas a simple task. This is not the case for the Si-SiC ceramic material used in the present work, though. The fracture surfaces of this material are completely uniform in appearance at both macroscopic and microscopic scales, making the boundary between the precrack and final fracture areas impossible to detect by direct observation. Because of the coarse grain structure of this Si-SiC (as compared to a pure, fine-grained alumina material, for example), there are no obvious macroscopic "chevron" marks on the surface to indicate crack growth direction, either. B&W attempted to locate crack initiation sites on their C-ring test specimens, both notched and unnotched, by searching for these markings. Three of the SC(B) specimens tested at INEL were also sent to B&W for examination. Even with high magnifications in an SEM, they could not reliably locate the initiation sites.

In order to detect the area of the precrack, techniques other than plain visual inspection were investigated. The first method tried was to infiltrate the precrack with an indicator solution that would dry prior to the actual testing, and then reveal the extent of the precrack once the toughness test was completed and the specimen was broken apart. Based on the surface length measurements of the precrack, the solution was not covering the full extent of the precrack area. The assumed problem with this method was that the precracks were so tightly closed, the fine solids in the solution were not able to reach to the tip of the precrack. Surface tension differences may also have been a factor.

The next procedure tried was similar to the heat tinting technique used in elastic-plastic test techniques. In this method, the precracked specimen is heated until an oxide film, which is a different color than the base material, develops over the precracked area. With the SiC material, it was found that heating to about 1250°C in air for 30 min caused a silica film (based on SEM analysis) to form on the specimen surfaces exposed to the hot air. This film, while not as revealing as the typical oxide films on metal specimens (steel or titanium, for example), does have a slightly different color appearance than the base material. The color variation seems to vary with film thickness, and ranges from a blue-gray color for thicker areas to a brownish-gray color in thinner areas. Although the color appearance becomes very thin and faint as the tip of the tightly closed crack is approached, and indeed may not reveal the entire extent of the crack, it does provide reasonable indication of the precrack length and relative curvature of the crack front. This method was used to verify the surface length measurements on most of the specimens with sharp precracks. Of all the specimens that were

a. Although a ceramic is being tested, it behaves as a very brittle, low toughness metal in the case of fracture properties (see Reuter et al., 1989, pp. 5-13). The validity requirements arising from elasticity considerations must still be met.

"heat tinted," there was good agreement between the heat tint crack length measurements and the prior measurements of precrack length described in the previous section.

5. FRACTURE TOUGHNESS TEST PROCEDURES

5.1 Fixtures and Alignment

Testing small-size specimens requires that extra care be taken in all stages of specimen preparation as well as in the test set-up to ensure accurate results. As the dimensions of the specimen to be tested get smaller, the dimensional and geometric tolerances of the specimen and the test fixture must be limited too, since errors in these dimensions are multiplied in the calculation of the final test results. Another factor to be considered in the testing of high modulus, brittle materials is the very small deformations involved during the test. Compare, for example, the testing of a more ductile metal specimen. The plasticity that occurs during the test tends to decrease the effects of specimen and fixture misalignment and dimensional inaccuracies. However, in testing small specimens of ceramic materials, the total deformations during the course of the test are very small. For a typical specimen tested in this program, the maximum mid-span (load-line) displacement is less than 20 μm. Special consideration was given to these factors to maximize the accuracy of the test results.

A special bend support fixture was constructed for the tests in this program (see Figure 6). The steel base was machined to very close tolerances, and included mounting for both a capacitive displacement transducer under the specimen mid-point and a linear variable differential transformer (LVDT) to measure the load-line displacement. The fixture has a fixed roller support span of 40 mm. A tilt adjustment fixture was designed and incorporated in the test set-up to provide precise alignment of the bend fixture support rollers with the loading ram. The tilt adjustment fixture consists of two circular disks about 15 mm thick and 150 mm in diameter, with a small variation in thickness across a diametral line (about 0.003 mm/mm) in both disks. When placed one on top of the other, small, precise changes of angle (less than 0.15 mrad) between the two outside surfaces are achieved by rotating the disks relative to one another. The disks can be rotated together to adjust the orientation of the maximum tilt angle. A hollow dowel pin in the center of the disks (press fit in one, loose fit in the other) keeps them aligned with each other, while allowing a draw bolt to pass through the disks to secure the bend support fixture to the load frame once it is aligned.

This support roller-to-ram parallelism adjustment is critical to obtain accurate test results. Because of the very small deformations involved, a very small error in setting this parallelism will cause the loading to be nonuniform across the specimen thickness. The resultant load shift towards one edge of the specimen can significantly increase the applied stress intensity in a localized zone near the crack's intersection with that surface (Figure 7). This increase can initiate crack extension at a lower applied force (than with a correctly aligned fixture), yielding a calculated fracture toughness (which is based on specimen geometry, applied force, and a perfectly aligned fixture) that is lower than the true value. This may be an explanation for some of the relatively large standard deviations in fracture toughness that were calculated in the Phase II testing.

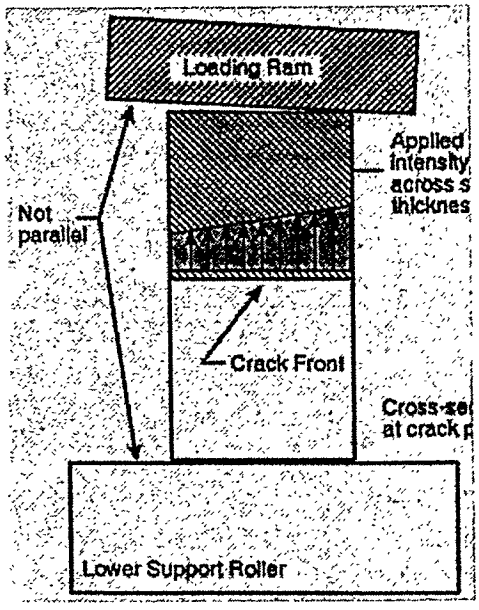

Figure 7. Diagram emphasizing errors due to fixture misalignment.

The procedure that was developed to achieve the precise alignment uses a specimen-sized hardened steel bar

that is surface ground to bring opposing surfaces parallel to better than 0.10 mrad. The long edges of the bar are given a light chamfer to remove sharpness. This alignment bar is placed in the bend fixture as a specimen would be. The loading ram is brought to bear against the bar in displacement control to achieve a small load of about 10-20 N. The bar is then translated parallel to the roller axis from front to rear while the load is monitored. Parallelism of the set-up is optimized when the variation of this force is minimized. Angular changes less than 0.5 mrad are quite noticeable using this procedure. Some testing has been done by others with a so-called "self aligning" bend fixture. The self-aligning features of these fixtures seem to be effective, but they also seem to have the drawback of being less rigid. For some testing applications, this may be an acceptable trade-off. However, for our testing, precise alignment combined with maximum rigidity were required to maximize crack growth stability (primarily for the precracking procedure). Other features of the crack growth process (described later in the section on Discussion of Results) were also observed that surely would have been missed if a more compliant test set-up had been used.

5.1.1 Notes on Fixture Alignment

In order for the precise parallelism set-up to be effective, the parallelism between top and bottom of the test specimens must also be carefully controlled. All of the specimens were machined by surface grinding and their parallelism was kept to better than 0.10 mrad.

The precracking procedure can be adversely affected by misalignment of the fixture, although the beam support precracking method (described earlier) should be less sensitive to misalignment due to the distributed support load under the specimen. Non-uniform loading (across the thickness of the specimen) created by fixture misalignment can cause the precrack to extend further on one side than the other (Figure 7, p. 20), which will invalidate the fracture toughness test results (E 399-90, 1991). This is especially true when any of the fatigue-type precracking procedures are used.

5.2 Fracture Toughness Testing Based on ASTM Standard E 399-90

Both notched and precracked SE(B) specimens of the Si-SiC material, described earlier, with nominal dimensions B = 5 mm and W = 10 mm were tested. The actual test procedure used to determine toughness generally followed the ASTM Standard E 399-90, except with regard to fatigue precracking the specimens and the use of a COD gage to monitor specimen displacement linearity.

Due to the extremely brittle nature of the Si-SiC material and its low toughness, precracking by mechanical fatigue is very difficult. Because of this, the beam support precracking procedure described in the previous section was employed.

A standard COD gage was not available that would fit the small ceramic specimens, so load-line displacement of the three point bend SE(B) specimens was monitored instead. The equivalence of the two measurements was discussed in the section on compliance-based crack length estimation.

The principle purpose of the fracture toughness testing performed in Phase III of the support program was to assess what, if any, differences in toughness measurements could be attributed to the relative sharpness of the notch/precrack in the specimen. All specimens tested prior to Phase III of the work had notches of varying root radii inserted using the EDM process, while the current work focused on testing specimens with sharp-tipped natural cracks.

The effect of the machined notch tip root radius was examined in detail in Phase II and reported by Reuter et al. (1989). The expected effect of increasing notch tip root radius increasing the measured value of toughness was observed and quantified. The Phase III work was performed to determine if a true fracture toughness (lower limit of critical stress intensity) was being approached asymptotically with decreasing root radius, specifically to the sharp precrack limit. From these results then, given the data scatter, a determination could be made whether the "true" fracture toughness could be adequately measured with a notched specimen.

Testing proceeded according to the requirements set in E 399-90, except the tests were performed at loading rates of about 0.10 MPa$\sqrt{m}$/s, which is less than the prescribed minimum 0.55 MPa$\sqrt{m}$/s. The reduced rate allowed improved time/load resolution of the AE data that were collected. It also allowed real-time observation of the load versus load-line displacement record. Small load drops caused by incremental crack extension became more apparent in this way. No detriment to the validity of the results were anticipated due to the lower loading rate. Rate sensitivity (over the range in question) is primarily associated with crack tip plasticity and localized stress relaxation, and this Si-SiC material has neither at the room temperature test conditions.

6. ASSESSMENT OF ENVIRONMENTAL EFFECTS ON THE FRACTURE PROCESS

The elevated temperature testing in Phase II of this program revealed several phenomena related to strength and fracture toughness that could not be explained at that time. EDM-notched test specimens that were exposed to 1250°C air for 30 to 100 min under no stress showed a small increase in room temperature fracture toughness.[a] Similar specimens held at the elevated temperature while subjected to an applied stress showed a larger increase in room temperature fracture toughness and an increase in fracture toughness at 1250°C. These apparent changes in material behavior would be beneficial for the proposed structural applications. However, the mechanisms causing the changes would have to be identified before the "improved" properties could be used in a design.

It was conjectured that changes in the material response in the notch tip region was responsible for the changes in fracture toughness. This may have been manifested by an actual change in K_{Ic} with environmental exposure, or physical changes in the material's structure, some combination of both, or some other phenomenon. The Conclusions of the Phase II report (Reuter et al., 1989) suggested that further investigation of the material's response to the high temperature air environment would be required to identify the mechanisms responsible for the observed phenomena. If they could be identified, a more solid base for the proposed design and assessment methodology could be provided.

The first possible reasoning for the behavior was that microcrack arrays were developing around the crack tip. These crack arrays would provide stress shielding at the notch tip. By the shielding mechanism, the remote stresses (applied forces) would have to be increased to achieve the critical stress required to initiate the failure at the notch tip. If the crack arrays were developing as a result of the high temperature air environment, it followed that application of stresses at the same time would serve to enhance the formation of the cracks and possibly enlarge the region where they developed. This could explain the observed toughening phenomenon. No cracks were observed (optical microscope and SEM) around the notch tip, with the specimens at room temperature and with no tensile loads applied. It was thought that observation at temperature and under applied loads may be more revealing. A high temperature moiré interferometry (HTMI) system that could measure localized displacements with high sensitivity was proposed for such an investigation. Development of such an HTMI system was undertaken as part of the Phase III work and is explained in a subsequent section.

Another idea that could explain the observed behavior involved creep mechanisms. Some siliconized SiC materials such as KX-01[b] do exhibit creep behavior at temperatures as low as 1100°C (see Carroll and Tressler, 1988). Extensive study of creep behavior of the KX-01 material has been done by Wiederhorn et al. (1988), Chuang and Wiederhorn (1988), Hockey and Wiederhorn (1989), and Chuang et al. (1991). The details of this work on phenomenology and creep deformation mechanics suggest a high probability of localized creep in the CS101K material, even though the Si metal content is less than for KX-01. Although the Si metal has some role in the creep process, movement of the SiC grains is the dominant factor. Another fact revealed in these references is an apparent tensile creep stress threshold. Below a certain stress, the creep rate is negligible, but at stresses slightly above the threshold the creep rate increases substantially. The work of Carroll and

a. A mean fracture toughness of 3.5 MPa$\sqrt{m}$ was determined based on results of three tests.

b. KX-01 Si-SiC, attributed to Standard Oil Engineered Materials Co. and Carborundum Corp. in separate references, has nominally 5 μm grains, 35% Si metal, and is fully densified.

Tressler (1988) put this threshold level at 132 MPa at 1100°C. Because of these factors, they also recommended doing creep experiments with specimens that had uniform stress distributions (tensile versus bend bars or C-rings, for example). All other parameters being equal, tensile creep rates were observed to be from 5 to at least 20 times higher than compression creep rates (Wiederhorn et al., 1988).

Based on these results, it is not unreasonable to expect localized tensile creep (at 1250°C) was occurring at the EDM notch tip in the SE(B) specimens tested during Phase II of this program. The hypothesis is as follows. Stresses are elevated at the notch tip, where steep gradients in stress also exist. Assume the SE(B) specimens are at a temperature that is high enough for the onset of creep behavior. Apply a remote bending load at a rate that is slow enough to allow creep to occur in the notch tip region. This allows locally high stresses to relax to (near) the creep threshold. Figure 8 depicts the elastic stress distribution prior to creep, and the possible resultant distribution after creep-induced stress relaxation. Further assume some critical stress state must be achieved to initiate fracture, and that this stress state is somewhat higher than the creep threshold. By lowering the stress level at the notch tip relative to the remotely applied load, an increased remote load (which is the basis of the reported toughness values in Phase II) would be required to initiate failure. This could explain the substantially elevated fracture toughness values reported in Phase II (Reuter et al., 1989) for specimens that were incrementally loaded at elevated temperature.

The Phase II work also indicated an elevation in room temperature fracture toughness for specimens that were held under load at elevated temperatures prior to the room temperature tests. This behavior is also consistent with the hypothesis. Assume that the creep and stress relaxation have occurred under load at temperature. The creep has been confined to a localized region surrounding the notch tip as shown in Figure 8, and is surrounded by material which is only elastically deformed. Upon release of the remote loading, the elastic body of material imposes a compressive stress on the material in the creep zone. But because (based on Wiederhorn's 1988 results for another Si-SiC) the compressive creep rate is so much slower, or the threshold stress much higher, the creep process is essentially unreversed even at elevated temperatures for moderate lengths of time. The result is a residual compressive stress field around the notch tip that exists from the moment the remote load is removed. This is certainly the case if the specimen is cooled below the creep threshold temperature at the same time the load is removed. Any subsequent testing would have the effects of the local residual compressive stress field (an unknown quantity) superimposed on the

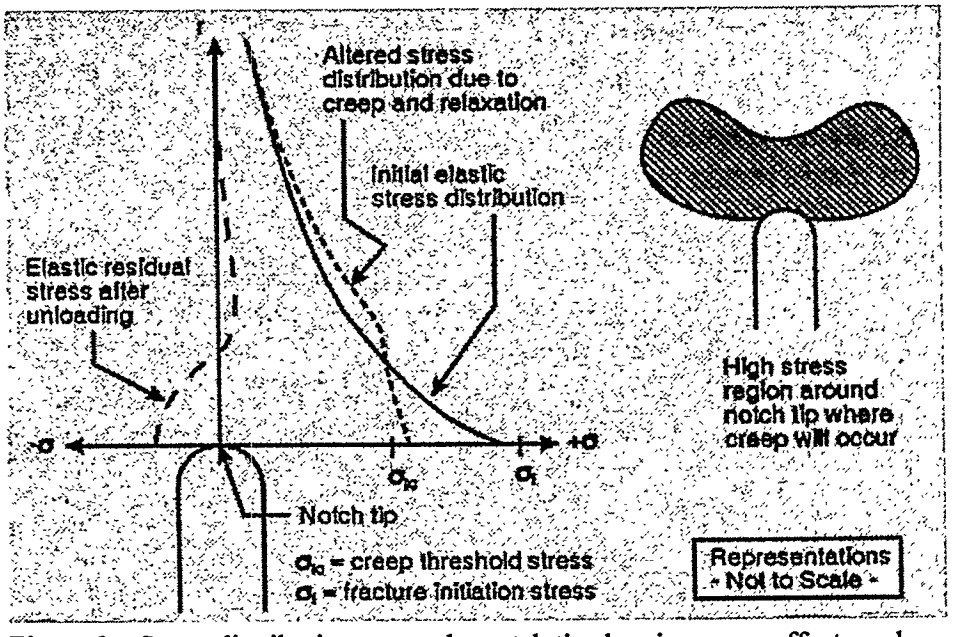

Figure 8. Stress distributions around a notch tip showing creep effects and affected region.

results. This would account for the elevated room temperature fracture toughness measured using specimens that had undergone the temperature-stress cycle.

The Phase II work did indicate a small increase (it may not be statistically significant) in room temperature toughness of specimens that saw a temperature-only cycle. The creep-based hypothesis would not account for this behavior. However, the microcrack array shielding of the notch tip could be a coincident mechanism along with the creep behavior. The work of Carroll and Tressler (1988) and Wiederhorn et al. (1989) described cavitation damage accumulation in the Si metal in the SiC intergranular spaces. At this point, Can cavitation damage really be distinguished from a microcrack array? Oxidation effects may also play a role in the observed phenomena. The development of the HTMI system was proposed to investigate the phenomena and determine the mechanism(s) responsible for them.

6.1 High Temperature Moiré Interferometry Development

Part of the research done in Phase III of this project was aimed towards development of a system to accurately measure displacements around the tip of a crack in a ceramic material at typical operating temperatures. At the time of the beginning of the Phase III work (late 1989), moiré interferometry had only been applied at temperatures of maybe 95°C, and then with great difficulty. It was hoped that during Phase III, the required technologies could be developed that would allow using the technique to temperatures approaching 1250°C. Three principal areas were identified that would require significant technological advances before the HTMI system, as the authors envisioned it, could become a working prototype. A diffraction grating to be applied to the specimen that would survive the elevated temperature environment would be required. An interferometer design capable of operating in close proximity to a hot surface (the specimen) would be essential. The elevated temperature environment would certainly produce distortions (due to convection and refractive index changes) in the interferograms (fringe patterns), requiring some method of reduction or correction. The following sections describe the development process for the HTMI system.

6.1.1 Moiré Interferometry Background

Moiré interferometry techniques have been developed for use at room temperature that have high displacement sensitivity (much less than visible light wavelengths), high range (several mm or more), and high spatial resolution. The technique uses a combination of coherent light (single wavelength, phase locked, as produced by a single frequency laser) and optical diffraction to make measurements. As it has been developed for room temperature applications, a high frequency diffraction grating (around 1000/mm) is replicated onto the specimen surface. Special epoxies or silicones are used in the replication. A thin layer of the material is bonded to the specimen, and the sinusoidal amplitude phase grating is replicated into it. A reflective coating is sometimes applied to the replicated gratings to improve the diffraction efficiency. The low moduli and small thickness (usually a few microns) of the replicating materials ensure that the replicated grating deformation follows that of the underlying specimen. Coherent light, in a pair of collimated beams (planar wavefronts), is used to illuminated the specimen grating. The angles of the beams are set so that equal diffraction orders (usually +/-1) emerge from the specimen grating parallel to each other. These wavefronts of the two diffracted beams interfere and a lower frequency standing wave is developed. This is the moiré interferogram that is collected and analyzed to determine the surface displacements. A complete discussion of the technique is provided by Post in Chapter 7 of the Handbook for Experimental Mechanics (1987).

The resolution and sensitivity capabilities of the moiré interferometry method make it highly desirable for investigating fracture mechanics and other crack growth phenomena, especially in ceramics where deformations are usually very small. However, limitations exist for the method's application at elevated temperatures (like those that are of interest in the investigation of structural ceramics). The whole concept of moiré interferometry has problem areas that must be overcome for its application at high temperatures. These technological hurdles include high temperature gratings, high temperature optical components, and optical design to handle or minimize perturbations of the coherent light beams caused by temperature gradients and convection currents (random refractive index variations along the beam paths). All of these topics were addressed in research carried out within the HTMI task in this program. The initial target temperature for this effort was 1250°C, the test temperature of the Si-SiC. After the initial investigation into the technique, the target temperature was revised to 900°C because of limitations encountered with the optical materials.

6.1.2 High Temperature Diffraction Gratings

An absolute requirement for a high temperature moiré interferometry system is a specimen grating that will survive at the temperatures of interest. This includes: (1) actual survival of the grating, and (2) that the grating retain sufficient optical properties, mainly diffraction efficiency. Existing methods of grating replication use an intermediate material bonded to the specimen, into which the actual grating is replicated. Professor Dan Post and Peter Ifju at Virginia Tech's Engineering Science and Mechanics Department assisted INEL in the development of a new "zero-thickness" grating replication technique (a concept report was provided in the Appendix of the Phase II report by Reuter et al., 1989). The basic concept uses a photo-resist material to produce a grating mask on the specimen surface. The initial work used a sub-micron thick reflective layer of gold sputtered onto a substrate. The photo-resist mask was developed over the gold film. The specimen is then placed in an ion milling chamber. The surface is then eroded away with ionized oxygen or argon bombardment. The resist mask, being softer than the metallic film, is eroded at a slow rate. The exposed gold film is eroded more rapidly. After sufficient ion milling exposure, a metal film bar and substrate space grating is left - an essentially zero-thickness grating. This system will survive without significant degradation to temperature exceeding 900°C. At room temperature, the diffraction efficiency is lower than a "standard" aluminized grating, but increasing the power of the illumination source can compensate for the reduced efficiency.

It was supposed that the above technique could also be used without the metal film coating. In the process, a phase amplitude grating (with ridges and valleys) would be created in the actual surface of the material. Such a grating would be able to survive as the material would. The primary concern would be the rate of oxidation or other surface degrading action of the elevated temperature environment. The ratio of reflectivity to emissivity of the surface at the temperature of interest would partially determine the quality of the resultant interferograms. The parameters for making a photo-resist mask of correct thickness and subsequent ion milling would have to be developed for each type of material, but it should be achievable. In the present research, the gold film gratings were produced on the polished surface of the CS101K Si-SiC material and room temperature moiré interferograms were successfully generated and recorded. The diffracted light intensity seemed to be about 5 to 10% of that expected from an aluminized, replicated phase grating. Appendix B in Reuter et al. (1989) details some of the early concept work commissioned by INEL and performed at Virginia Tech on zero-thickness gratings.

During Phase III, several Si-SiC specimens were prepared with the gold film, zero-thickness gratings for future use with the HTMI system. Both plain and notched specimens were produced with these gratings.

6.1.3 Interferometer Design

There are many factors involved in the development of an optical interferometric device that will operate at elevated temperatures. The component materials that will be used in the high temperature zone must be able to withstand the temperatures without degradation. Some components will require either highly reflecting, partially reflecting, or anti-reflection coatings on their surfaces. These coatings must withstand the high temperature environment, too. Given that the interferometer will most likely be immersed in a gaseous environment, the role of convection (leading to nonuniform refractive index due to temperature gradients) must also be considered. These factors were considered and the following interferometer design was developed in conjunction with Prof. Post.

The primary quality of the interferogram that is produced by an interferometer is influenced by the quality of the two beams used to produce the interference pattern by way of the diffraction grating. These two beams must always travel through some different part of space prior to impinging on the diffraction grating, because they must impinge at two different angles. From where a single beam is split and begins traveling on two separate paths is referred to as the non-common path and the relevant distances traveled are referred to as the non-common path lengths. Perturbations in the collimated illumination beams that occur independently in the non-common paths provide for the largest irreconcilable degradation of the interferogram that is produced. For an interferometer that operates in an elevated temperature gaseous environment, convection currents on the non-common paths create substantial degradation of the system's performance. With this in mind, an interferometer with minimum (small) non-common path length (outside of solid optical elements) was devised. A system of optical elements was designed to produce the desired beam angles at the specimen's surface. A plan view schematic of this interferometer is shown in Figure 9.

As can be seen in the diagram, the non-common paths external to the optical elements are limited to two narrow gaps. One is between the prism element and specimen, the other between the prism and the frequency adjustment mirror. The design has an adjustment feature that allows for precise frequency adjustment to compensate for thermal expansion of the specimen and refractive index change of the prism components. The proposed design would have specimen coverage over an area a bit larger than 10 x 10 mm. It should not be too difficult to enlarge the elements to provide a larger coverage area.

The optical elements of the system are specified to be fused silica. This material should be stable to at least 900°C. If a prototype system of the fused silica material demonstrates feasibility, a system could be developed using sapphire (although birefringence could be a problem) for higher temperature operation. Multilayer dielectric coatings are specified for antireflection and partly reflecting surfaces. The dielectric coating vendors specify an allowable temperature of 400+°C for the antireflection coatings. The vendors have successfully tested them to 600°C using relatively slow, controlled heating and cooling rates. The thicker partial reflection coatings have not been tested to these elevated temperatures by the vendors. A sample optical flat with a 30% reflecting multilayer coating has been tested to 400°C without showing any damage.

Figure 9. Schematic diagram of high temperature moire interferometer showing essential optical elements and beam paths.

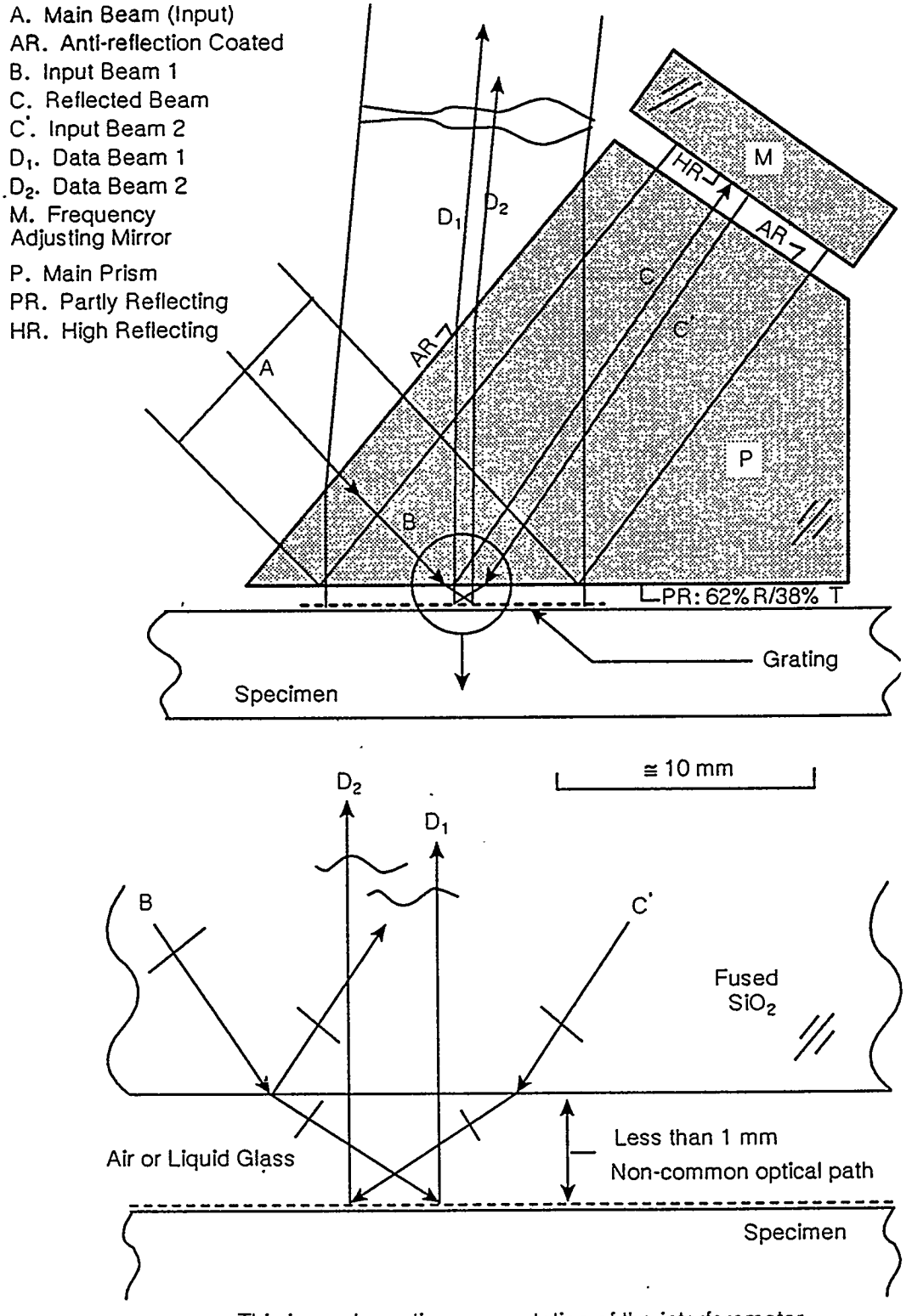

This is a schematic representation of the interferometer. Dimensions and angles are not drawn to scale.

The adjustment mirror surface has not been specified, but its temperature should be low enough that a coated metal film surface should work (some type of refractory metal may be required).

There is some concern about the temperature gradients that will exist in the main prism, since the system will be radiantly heated from one side by the specimen. The resultant temperatures will be nonuniform in the prism, although the degree of nonuniformity is not known. Deformation of the optical surfaces, due to the thermally-induced strains, is another potential problem. Since the temperature profiles are not known, the resultant gradient of refractive index inside the prism may cause some problems. If the gradients are not too large, and not changing too rapidly (i.e. near steady state), there may be ways to process the interferograms to compensate for the resultant nonuniformities. In the event that the gradients are too large to be tolerable, it may be possible to heat the whole interferometer system to a near constant temperature closer to the specimen temperature. However, this solution may have the drawback of increasing the convection currents surrounding it, further degrading image quality.

By keeping the gaps between the elements small compared to the planar sections, a relatively constant temperature should be achieved within the gaps. By stabilizing the temperature, convection in these volumes will be minimized. If these volumes can be fully enclosed, convection currents could be practically eliminated. This should help the stability of the resulting interferograms. Another possible solution to convection currents in the gaps would be to use a liquid couplant (such as soda-lime glass at the temperatures of interest) between the interferometer and the specimen. This could virtually eliminate convection in the hottest regions, but a prism body with different angles (or different specimen grating frequency) would be required because of the refractive index change from air to liquid glass.

The optical elements of the proposed system would be mounted on ceramic rods that lead to precision kinematic mounts outside of the hot area. The mounts would provide adjustment of the prism relative to the specimen and of the frequency adjustment mirror relative to the prism. It is envisioned that the whole interferometer system will be mounted to the test frame adjacent to the specimen mounts outside of the hot area. The initial application for the system was to be assessment of notch and crack tip behavior of Si-SiC bend specimens. The SiC specimens were to be inductively heated, since SiC is inductively susceptible. This would minimize direct heating of the dielectric optical elements to only that caused by the specimen's irradiance.

Although a prototype interferometer was not constructed, the basic design has been completed. Most of the technical questions have been addressed and what are thought to be suitable solutions to them proposed. If funding becomes available in the future to resume this development, the remaining unknowns will be assessed and an operating prototype will be constructed. At this time, it is anticipated that only a moderate amount of funding would be required to follow through the prototype development.

6.1.4 Image Processing of the Moiré Fringe Patterns

It is certain that fringe patterns produced by the HTMI system will be of substantially lower quality than a typical room temperature interferogram. A general reduction in fringe contrast will arise from the basic design of the proposed interferometer, due to the unequal beam intensities produced by the partial mirror and prism beam splitter. This is an unavoidable consequence of the basic design. The fringe images will be further degraded by convection currents and distortion of the optical elements resulting from nonuniform temperatures. These are all basic problems associated

with the elevated temperatures. A further concern is the relatively small displacements that are expected to occur at and around the crack or notch tip in the ceramic materials. Based on room temperature tests of the Si-SiC material, as few as two to three fringes may be all that can be expected, even at loads approaching failure. The combination of relatively poor image quality combined with only a few fringes to analyze calls for some means of improvement. The proposed solution will use a variety of image analysis techniques. They would be selected and employed based on the actual requirements for "clean up" of the raw interferograms.

6.2 Stress Corrosion Cracking (Static Fatigue) in 1250°C Air

Since one principle application of this Si-SiC material is in heat exchangers in steel production plants where the material is exposed to high temperature air and combustion by-products, the effects of such an environment on the fracture behavior of the material is obviously of interest. In the Phase II work on this project, specimens with EDM notches were subjected to a fixed bending load for various periods of time at 1250°C. The longest exposure was for about 1000 h at an applied stress intensity factor of about 95% of the nominal material fracture toughness at 1250°C. The results of this work indicated that there was no detrimental effect (stress corrosion cracking was the primary concern) due to the high temperature air environment (Reuter et al., 1989). Instead, it appeared as if exposure to 1250°C air while under an applied stress increased fracture toughness. A test program was planned that called for further long term testing up to 3000 h in conjunction with tests utilizing the capabilities of the HTMI system just described. This portion of the Phase III effort was plagued with difficulties. As mentioned above, an operating prototype of the HTMI measurement system was not completed, so the associated investigation of the crack tip behavior at elevated temperatures could not be performed. Problems also occurred in the long term testing program, and they are described below.

During Phase III, the program plan called for duplicate tests for a significantly longer duration. A few EDM-notched specimens were to be tested for up to 3000 h in order to add additional data to the existing set (shown in @@Figure 10). Afterwards, some sharply precracked specimens were to be tested in the same set-up. This would provide a basis for assessment of environmental effects on real component tubes that contained cracks or crack-like defects. The stress corrosion testing furnace used in Phase II was renovated and set up for the 3000 h test. The specimen loading apparatus was redesigned for improved loading accuracy. Where the old system used in Phase II work had a cantilevered loading arm and bronze pivot bushings, the new one used direct load application over the loading ram and steel roller bearings at all pivot points. Loading for both systems was by dead weight application; usually a combination of cast iron weights and lead shot were used to achieve the desired load. A new thermocouple and temperature readout were acquired to verify furnace and specimen temperature. The same alumina three-point bend support used in Phase II work was reused.

An EDM-notched specimen was aligned in the loading fixture with a small preload applied. The furnace was brought to operating temperature and the specimen was soaked for 30-45 min. The required final load was precalculated based on specimen geometry, notch depth, and the desired stress intensity level of 95% of K_{Ic} at 1250°C. This amount of weight was premeasured in lead shot on a precision electronic scale. The load on the bend specimen inside the furnace was slowly increased by adding the premeasured lead shot to the weight pan (of course the preload was included). The first specimen failed during the initial loading at about 85% (exact load unknown) of the expected failure load based upon the mean value of K_{Ic} at 1250°C.

Since the material had a fairly large standard deviation for K_{Ic}, a statistically weaker specimen was suspected for the premature failure. The entire system was carefully checked after the second specimen failure at 80% of the expected failure load. No defects, systematic errors, or other faults were found. A normal elevated temperature fracture toughness test configuration was set up and three duplicate EDM-notched specimens from the same tube segment were tested for confirmation of KIc at 1250°C. The tests validated the previously measured mean value of KIc at 1250°C to be 3.8 MPa√m.

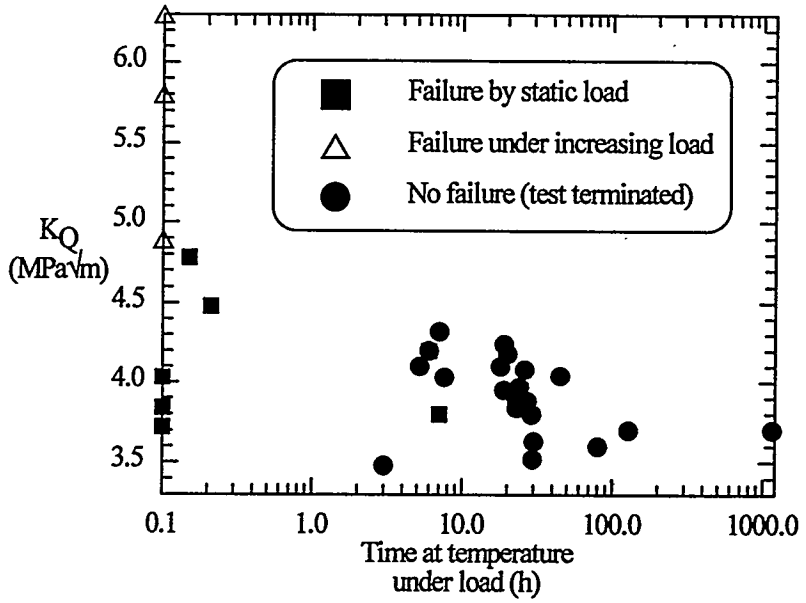

Figure 10. Applied stress intensity factor as a function of time for CS101K tested at 1250°C.

The set-up and initiation process for the long-term test was repeated three more times, and premature failure of the specimen during initial loading occurred each time. The failure loads ranged from about 90% down to 58% of the expected failure loads for these remaining specimens. The lowest value was near the lower limit of fracture toughness at room temperature, and was the lowest value of K (although not a valid fracture toughness measurement) recorded for any of the specimens tested at 1250°C. At this point all EDM-notched specimens reserved for the long-term testing had been used up. Because of unresolvable problems with the (apparently) long-term elevated temperature test system, this task was suspended.

6.3 Multiple Crack Interaction Effects on the Fracture Process

A sub-task of the Phase III portion of this program was to investigate crack tip interaction effects on the fracture process for closely-spaced crack tips. More accurately stated, the investigation was to focus on the possible development of smaller cracks in the immediate vicinity of the main crack tip and their resultant effects on toughness. This effort was motivated by the observed increases in toughness detailed by Reuter et al. (1989) in the Phase II report, and the subsequent hypothesis that the phenomenon may be caused by some type of crack tip shielding process. Moiré interferometry is a particularly useful investigative technique for this type of mechanics problem. It allows the displacement fields around the crack tip to be accurately mapped. Analyzing these fields can reveal small (or large) perturbations from the known linear fracture mechanics field solutions. The high temperature moiré interferometry system would have been used to examine the crack tip region for these variations, if an operational model could have been developed.

It was thought that it may have been possible to synthesize test specimens with multiple cracks that were closely spaced for use as benchmarks in the investigation. As it turns out, it was very difficult to generate the single-edge-cracked specimens required for the main task. At one time, it was hoped that the bridge-indentation method may be able to produce some of these specimens, but

the attempts failed. A crack always popped-in from one of the multiple indent starter defects, which apparently immediately "shielded" the other indent sites so that the required pop-in stress was never reached. At no point could a specimen with multiple cracks be produced. Since no suitable specimens could be made, multiple crack interactions, or crack array shielding effects, could not be investigated experimentally.

7. DISCUSSION OF EXPERIMENTAL FINDINGS

7.1 Precracking Procedures

The two precracking procedures used during this work, the bridge-indentation method and the beam support method, both appear to be viable alternatives where a sharp precrack of relatively large size is required. The present work suggests that the beam support precracking method may be a better choice for the siliconized silicon carbide tested in this research. The beam support method has several advantages over the bridge-indentation method. A simple three-point bend fixture is all that is required for loading, where the bridge-indentation method requires special fixturing. The specimens used in this program for beam support precracking had starter notches inserted with EDM, but a narrow saw cut using a diamond wafering saw should work just as well. A saw cut would be required for using this method on the many non-conductive ceramic materials that could not be machined using EDM. The beam support method allows for controlled crack extension of the precrack, where the bridge-indentation method relies on controlling the size of the starter defect to approximately fix the size of the final pop-in precrack.[a] The beam support method does have the one drawback that the precrack length produced is not predetermined by applied load or some other external factor. The precrack length must be assessed at intermediate stages of the precracking process until the desired length is obtained. However, for the present work, the beam support precracking method performed well and produced excellent sharply-cracked test specimens.

7.2 Fracture Toughness Testing Using Sharp Precracks

7.2.1 Stable Crack Growth

Stable crack growth was observed following crack initiation in every precracked specimen during toughness testing. A representative plot of applied force versus load-line deflection is shown in Figure 11 (p. 34). Acoustic emission monitoring was used in some of the tests. No substantial amount of crack growth was detected with AE until just prior to the first pop-in load being reached. The gradual load drop following maximum applied force is indicative of the stable crack extension. A crack growth resistance (R-curve) analysis was not performed, but the nature of the force/displacement curve suggests a slightly rising R-curve for the precracked Si-SiC specimens.[b] The slightly rising crack growth resistance may be a property of the CS101K material. It may not have been noticed in the tests of the EDM notched samples due to the different stress distribution around the notch tip compared to a sharp crack. The crack initiation event is triggered by some critical stress level being reached over some volume of material. The finite radius of the EDM notch causes a lower gradient in the stress field surrounding it. When the critical stress at the notch tip is reached, the stresses in the surrounding region are higher. This leads to the instability observed in the tests of EDM-notched SE(B) specimens. However, the gradient in stress near the crack tip is higher for the sharply cracked specimens. Less crack driving energy is available as the crack extends, leading to the quasi-stable extension. This hypothesis is based on known characteristics of the

a. Some work has been done by Prof. Isa Bar-On using a reversed (compression) bending fatigue process to straighten uneven length precracks. It is not known how effective this method may be for extending an initially straight precrack.

b. Crack growth resistance and most R-curves that describe the phenomenon are known to be geometry-dependent in most cases. The behavior observed in this work was limited to SE(B)-type specimens of the CS101K material. Other specimen geometries may give different results for the same material.

stresses around notches and cracks, and the fracture initiation mechanisms in brittle ceramic materials.

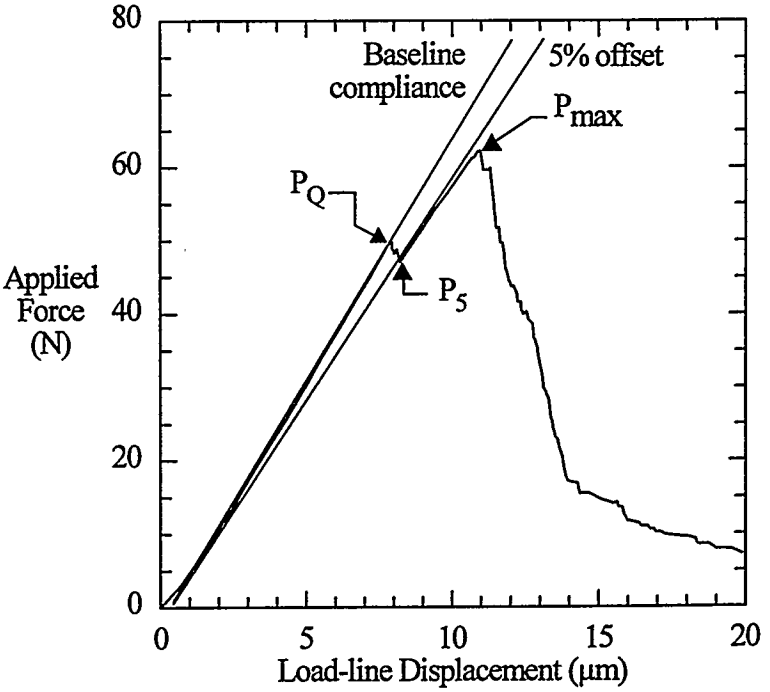

Figure 11. Representative load versus load-line displacement curve for precracked Si-SiC (#2K-08).

It is not known whether this phenomenon is partly responsible for the observed increase in measured toughness for the precracked specimens. A complete assessment of crack growth resistance for the material may provide some of the answers. If the R-curve rises more than presently expected, it may explain, to some extent, the substantially elevated values of fracture toughness measured with the SE(B) specimens. The ones having the longer precracks yielded higher values of toughness than did the specimens with shorter precracks. The crack growth mechanism during the beam support precracking procedure is no different than during the actual testing; the energy release rate is just suppressed by the support beam. Therefore, any subsequent crack growth from the precrack should be equivalent to additional extension from an existing crack having grown from zero length to the same length as the precrack. A rising R-curve type of material behavior could explain the higher values of K that the longer cracks produced.

7.2.2 Elevated Toughness Values at Room Temperature

The results of the first two tests of the sharply precracked (using bridge-indentation method) specimens gave toughness values of 5.42 and 4.35 MPa$\sqrt{m}$. These specimens had not been exposed to elevated temperatures for "heat tinting" the crack surface or any other environment expected to elevated the material's toughness. These values were significantly higher than the expected lower limit fracture toughness of about 2.9 MPa$\sqrt{m}$, based on the EDM-notched specimen data. The test fixturing, instrumentation, and data analysis were all closely scrutinized for possible sources of error in the results. No errors could be detected, so additional specimens were tested for verification, and yielded equally elevated values of K_Q. Table 3 and Table 4 show the results of these tests.

Table 3. Beam support precracked specimen toughness data.

Specimen #	2K-08			2K-09			2K-20		
Thickness, B (mm)	4.97			4.99			5.08		
Width, W (mm)	6.46			7.98			8.81		
a/W: EDM notch	0.536			0.522			0.527		
Δa/W (precrack) avg at surface	0.060			0.135			0.381		
Δa/W (precrack) avg of heat tint	0.040			0.065			0.360		
Total a/W (surface)	0.596			0.657			0.908		
Total a/W (heat tint)	0.576			0.587			0.887		
	Pop-In	P_Q	P_{max}	Pop-In	P_Q	P_{max}	Pop-In	P_Q	P_{max}
Applied Force (N)	50.1	50.1	62.5	66.9	66.9	74.9	≈24	26.2	29.5
K using a/W (surface) (MPa√m)	--	2.88	3.59	--	3.59	4.02	7.99	8.72	9.82
K using a/W (heat tint) (MPa√m)	--	2.68	3.34	--	2.70	3.02	5.85	6.39	7.19

Table 4. Bridge-indentation precracked (INEL) specimen toughness data.

Specimen #	Surface Measurement		Compliance Estimated	
	a/W	K_Q (MPa√m)	a/W	K_Q (MPa√m)
2J-03	--	--	--	5.42
2J-04	--	4.78	--	4.35
2J-10	0.292	--	0.247	4.79
2J-11	0.271	5.45	0.251	5.19

Crack Face Roughness Effects. A hypothesis was formulated that explained the elevated toughness values (and potential rising R-curve behavior previously discussed). Crack face surface tractions, due primarily to frictional forces on the rough crack faces, provided an effective internal crack closing force. However, this closing force cannot be measured directly by experiment. An experimental plan was developed to test this hypothesis by indirect means. Specimens with equal length EDM starter notches (a/W~0.5) were precracked to varying final crack lengths (a/W~0.55-0.75), giving sharp precrack lengths from 0.5 to about 2.5 mm. Accurate stress intensity calibration equations for edge-cracked bend specimens with cracks in this length range are available in *The Stress Analysis of Cracks Handbook* (Tada et al., 1973). The equation for the three-point bend specimen with span to width (S/W) ratio of four is:

$$K_I = \frac{3\,P\,S\,\sqrt{\pi a}}{2\,B\,W^2}\left(14.57\left(\frac{a}{W}\right)^4 - 14.18\left(\frac{a}{W}\right)^3 + 8.20\left(\frac{a}{W}\right)^2 - 1.735\left(\frac{a}{W}\right) + 1.090\right) \quad (1)$$

with a specified accuracy of 1% over the full range of crack lengths (a/W = 0.0 to 1.0). Note the solution in Tada et al. is for a specimen of unit thickness, so the right side of equation is divided by specimen thickness, B, to account for actual thicknesses other than 1. Plasticity and corresponding plastic zone size is not a concern in this material, so the remaining ligament size (b = W - a) can be quite small and still give valid results. Any significant effect due to superposition of the local compressive field caused by the three-point bend loading ram ahead of the crack tip is also unlikely, given the low applied forces and the high elastic modulus of the Si-SiC. So, the varying precrack lengths provided varying amounts of potentially interacting rough crack surface area, and varying distances of interacting material behind the crack tip.

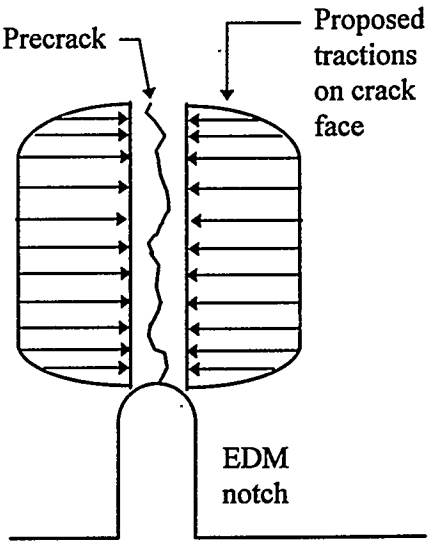

Figure 12. Schematic diagram of notch and precrack showing crack face tractions reducing the actual crack tip stress intensity factor.

Figure 12 shows a schematic diagram of the typical specimen, the hypothesized forces, and where they act to produce the observed behavior. As can be seen in this figure, the proposed internal surface tractions acting on the crack faces would serve to provide a resistance to crack opening (effectively superimposing a negative bending moment at the remaining ligament). These forces would counteract the positive moment (crack opening force) induced by the external three point bend loading. Although the distribution of the surface tractions is unknown, assuming them to be approximately uniform is not unreasonable for the initial test verification. Taking this to be the case, more rough crack surface length behind the crack tip would provide a higher ratio of resisting moment as compared to the remotely applied moment (bending force) than a shorter length of rough crack surface. These specimens were then tested in the normal manner, and the results were analyzed.

The test results are presented in Table 3 (p. 35), and, based on the stated hypothesis, confirm that a significant alteration of the measured fracture toughness is caused by the interaction of the crack faces behind the crack tip. The shortest natural crack yielded a toughness value that was the same (given the relatively large standard deviation of toughness developed from Phase II data, as shown in Figure 13) as measured with EDM notched specimens. The longer natural cracks had the highest measured values of toughness, and the intermediate crack lengths had intermediate toughness values. These results are very significant.

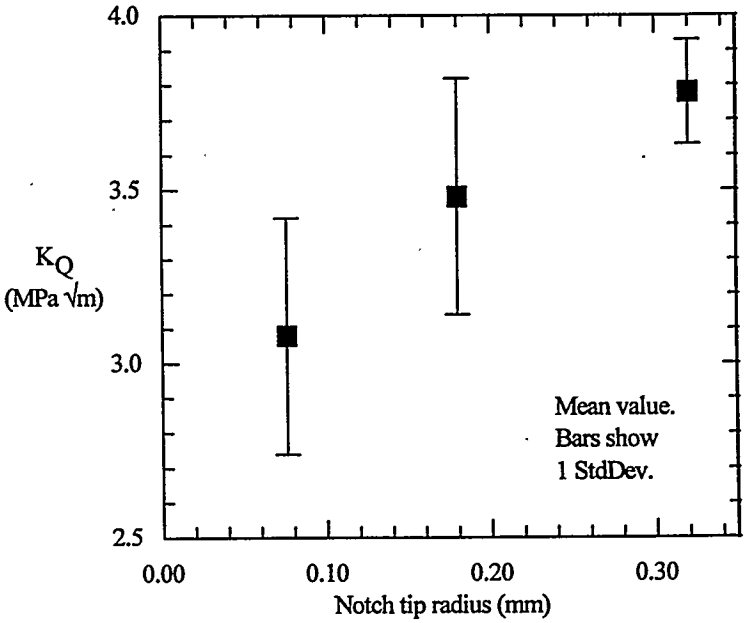

Figure 13. Measured fracture toughness of CS101K as a function of EDM notch root radius (20°C).

They point to a substantial increase in apparent toughness for longer cracks, that would provide a "built-in" factor of safety in a fracture mechanics-based design using the actual fracture toughness of the material.

An alternative approach to prove the hypothesis would be to use moiré interferometry to measure the displacement fields in the local region around the crack tip. These data can be analyzed to determine the actual stress intensity factor at the crack tip, independent of the specimen geometry and the applied forces. By making such measurements, the portion of K attributable to the crack wake can be separated from the part due to the remotely applied load, as $K_{wake} = K_{moire} - K_{load}$. The requirements for the assessment by moiré are relatively simple. The material elastic properties are needed, and the crack tip cannot be too close to a free boundary on the specimen. One difficulty in analyzing the Si-SiC material this way is the small displacements of the material around the crack, that only provide a few fringes on the interferogram. However, a technique called phase shifting can be used to enhanced the sensitivity (displacement resolution) of the technique to better than 10 nm, or about 1/50 of a wavelength of the laser light. A combination of phase shifting and high image magnification to boost the spatial resolution would allow the most direct assessment of crack face roughness effects on measured fracture toughness. A phase shifting interferometer was not available at the time that this experimental work was being performed. However, an automated phase shifting system with integrated video fringe pattern acquisition and analysis has been developed at INEL and is now available for this type of experimentation.

The results of the indirect experiments do provide verification of the phenomenon, if not absolute proof of the hypothesis. Regardless, potential catastrophic failures (governed by fracture mechanics principles) in structural applications of this material (such as the aforementioned heat exchanger system) will likely be preceded by some amount of stable cracking in the structure. If this is the case, a fracture-resistant design based on the lowest measured toughness, the "true" K_{Ic}, will provide some built-in safety margin, since the crack surface interference (or effective rising R-curve behavior, if you like) will serve to effectively elevate the material's toughness.

There was no indication, based on the tests of the shortest sharp precrack lengths, that the true fracture toughness of this Si-SiC material could not be correctly determined by testing the EDM-notched specimens (without a precrack). Therefore, the toughness values measured using the EDM-notched SE(B), A(B), or even externally notched C-ring compression specimens should be adequate for design purposes. Remember, however, that scatter (measured standard deviation) in the measured toughness values increased for the A(B) and C-ring specimens. Because of this, an additional number of specimens would need to be tested to obtain a reliable mean value or lower limit of fracture toughness.

The additional details associated with the observed sharp crack phenomena certainly merit additional research. They include an accurate assessment of the mechanism of the resisting surface tractions in the natural cracks, effects of cyclic fatigue on the resisting forces provided by the crack face roughness, and environmental effects on the sharp, natural cracks. In the time since these phenomenon were first observed and investigated, INEL has advanced its experimental capabilities. Many of the suggested approaches for these advanced investigations could now be accomplished at INEL, however there are substantial hurdles remaining to be crossed before the high temperature moiré interferometer, or HTMI, will be a working research tool. Such experimental work will further the understanding of the fundamental mechanics of this class of material. By applying the results, new, safer, or more reliable applications of the material could be accomplished, e.g. by allowing further weight optimization of structural designs while maintaining acceptable reliability.

Microcrack Shielding of the Crack Tip. Early in this investigation, and in subsequent discussions with others doing research in this area, the topic of crack tip shielding by arrays of microcracks surrounding the main crack tip was discussed. Earlier, the possible effects of microcracks around the EDM notch tips was a concern. As mentioned before, an SEM investigation of the EDM notch tip region did not reveal any microcracks. After the results of the first sharp crack toughness tests showed the substantial elevation of toughness, it was postulated that microcrack damage may be responsible for the observed behavior. The subsequent tests with varying length cracks, all produced by the same method, discredited this postulate. Each specimen would have an equivalent zone of microcrack damage (if it does exist) surrounding the crack tip, since the cracks were produced in the same way. Yet the dominant factor with best correlation to the toughness change was the length (area) of the sharp crack. These results do not point to significant microcrack damage in the Si-SiC material contributing to crack tip shielding, with an apparent toughness increase as the result. However, even if there is some microscale damage, its effects would be included within the test results that were obtained.

This work focused primarily on fracture behavior on the macroscale, i.e. failures that could be attributed to relatively large cracks or crack-like defects. The methods of investigation relied on the basic concepts of linear elastic fracture mechanics. Because of these assumptions, any affects that may result from microcrack phenomena would be accounted for in the toughness measurements that were made, and would appear as an intrinsic part of the measured toughness properties of the material. Then, whether a test specimen or a structural component, the response should be predictable based on the measure fracture toughness properties.

Combined Environmental Effects. The long-term stress corrosion cracking (static fatigue) tests that were planned for Phase III to enhance the data developed in Phase II were not successful, as explained in the earlier section on Stress Corrosion Cracking. The inability to complete the development of the HTMI system also hampered the research effort. Because of these problems, it is not possible to explain, with certainty, the lack of material degradation (stress corrosion cracking, static fatigue, etc.) or why the material showed increases in fracture toughness after exposure to combined temperature and stress. The most significant possibility considered was a localized creep mechanism, which was discussed in the section on Assessment of Environmental Effects on page 23. Because this mechanism would be highly localized in its action, the global measurements of displacements and the visual examinations of the specimens would be ineffective in isolating it. Use of the HTMI system, if it could have been completed, may have provided additional insight into the creep hypothesis because of the high spatial resolution and fine displacement sensitivity. The HTMI system may also have been used to determine local crack tip stress intensity values as a function of time at temperature under fixed loading conditions. These factors and others described earlier did not allow experimental data to be developed beyond the 900 h limit obtained in the Phase II work. Because of these circumstances, the lifetime prediction capability for this Si-SiC material cannot be reliably extended beyond 900 h at this time. Some possible mechanisms that may be in effect have been identified, and a rational explanation provided, although without absolute verification. A small to moderate amount of testing may provide the missing keys to verify the hypotheses, which could then be used to extend the lifetime prediction capabilities for this material.

8. CONCLUSIONS

A great deal of new knowledge was developed and experience gained throughout the course of this program to provide support to the "Assessment of Strength-Limiting Flaws in Ceramic Heat Exchanger Tubes" being conducted by B&W.

1. Based on the results of fracture toughness tests using both EDM-notched and sharply precracked test specimens, the fracture toughness values measured using the EDM-notched SE(B), A(B), or externally notched C-ring compression specimens should be adequate for design purposes, provided enough specimens are tested to establish reliable mean values and lower limits. To further reduce costs, saw-cut notches possibly could be used in place of the EDM notches. Regardless of the notching method, the uniformity of the notch root would need to be controlled and the absolute size and shape of the tip should be semicircular with a maximum radius less than 75 μm.

2. A new method for introducing sharp-tipped precracks in brittle ceramic materials was developed. It was used to successfully prepare SE(B)-type fracture toughness test specimens for the Phase III portion of this project.

3. Results of the sharp crack toughness tests showed a variation in measured toughness with precrack length. This led to the hypothesis that crack wake interference was affecting the toughness measurements. Subsequent tests showed a correlation between length of precrack (crack area) and measured fracture toughness. Because of this, toughness measurements obtained from precracked specimens with relatively long crack lengths should be carefully assessed for validity. Toughness measured this way may be artificially elevated.

4. An apparent rising R-curve behavior, that is, fracture toughness appears to increase with increasing crack growth, was noted during fracture toughness testing using the sharply precracked SE(B) specimens. This behavior was not quantified by actual R-curve tests, but the load versus displacement relations recorded during the fracture toughness (E 399-90) tests indicated that type of behavior. This observation is consistent with the evidence and conclusions of (2) above.

5. If the postulated crack wake interference can be shown to exist in cracked structures, it may provide an additional degree of structural safety if a true lower limit fracture toughness is used in a fracture mechanics-based design or assessment.

6. The test results obtained indicate little effect of a 1250°C air environment on fracture behavior, i.e. cracking processes, of the CS101K siliconized SiC material. Time at temperature and stress do not appear to effect actual crack growth in this material at the temperatures and stress (stress intensity) levels investigated, although an apparent elevation in the material's fracture toughness was observed after the combined temperature/stress exposure. It is believed that a localized creep phenomenon may be responsible.

7. All elevated temperature data was obtained from EDM-notched specimens, which present an open volume at the notch tip. This open volume allows the environment direct contact with, and easy circulation to, the notch tip. Care should be used in inferring behavior of sharp cracks based on these data. If the environment is affecting the crack growth process (at the crack tip), a more tightly closed crack may lessen the effects, e.g. restricting oxidation of the near-tip surfaces. Conversely, if there is a synergism between the environment and crack tip stresses, the potentially higher stresses at a sharp crack tip (compared to a blunt notch) may enhance and accelerate environmentally-assisted cracking, e.g. a stress corrosion cracking mechanism.

8. The database of effects of temperature and applied stress intensity on slow crack growth (stress corrosion cracking, static fatigue, etc.) is still limited to exposures of 1200 h or less. The inability to complete the development of the high temperature moiré interferometry system precluded attempts to quantify the actual stress intensity factor at the notch or crack tip at elevated temperatures.

9. A methodology for making conservative (safe) predictions of critical flaw sizes in Si-SiC ceramic tube components was developed. The predictions are accomplished by using measured fracture toughness values (from standard fracture toughness specimens with EDM notches), the Newman and Raju (1979) equations for stress intensity distributions around semielliptical surface cracks, and realistic estimates of the applied stresses (or design allowable stress) the component will experience. The conservatism of the predictions made using this methodology are increased for crack-like defects, based on the results of the sharp crack tests made in Phase III. This is based on the observations that the EDM-notched specimens provide a minimum valuea of fracture toughness, and that "real" cracks (sharp-tipped with rough, interacting faces) show an effectively higher toughness with increasing crack growth resistance as the crack extends.

---

a. This minimum toughness value could be any of several values, as determined by the criticality of the application. The actual value, based on a given data set, could be either the mean, the absolute minimum, a lower limit based on a specified confidence level, or any relevant and reproducible value based on the known data.

9. SUMMARY AND RECOMMENDATIONS

9.1 Project Summary

The Phase III support work had two objectives to be met: (1) determine the effect of test specimen notch/crack geometry on the measured fracture toughness; and (2) assess the effect of the operating environment on the material's fracture toughness over time (property degradation). To meet these objectives, specimen preparation techniques were developed, test procedures were developed, specimens were tested, and results were analyzed.

The "beam support" method for brittle specimen precracking was developed. This technique allows sharp-tipped precracks to be inserted into the coarse-grained, monolithic CS101K ceramic material. Reasonable control over the final length of the precrack is maintained using this technique. The technique could be applied to any very brittle material that is difficult to precrack by the normal fatigue methods (including most monolithic ceramics, some ceramic composites, glasses, etc.).

The beam support precracking technique was used to produce a number of test specimens with sharp cracks, as may be found in actual structures. These specimens were tested and the fracture toughness was determined from the test results. The measured fracture toughness was found to be considerably higher than the values obtained by testing specimens with narrow EDM notches. Longer precracks, with more crack face area to interact, had higher measured toughness values. The interaction of the crack faces was determined to be the cause of the elevated toughness values. This conclusion was based on the varying results of tests of specimens with varying precrack lengths, and hence crack face area.

Specimen testing for extended times in an air environment at 1250°C did not yield any results that suggested degradation of the material's toughness. Conversely, a possible localized tensile creep process was hypothesized to be the cause of an apparent rising fracture toughness over time with combined exposure to elevated temperature and tensile stress in the crack tip region. The fracture toughness measured at 1250°C by standard tests using EDM-notched specimens is elevated over room temperature toughness about 20%. The additional toughness due to the hypothesized behavior (crack face interaction and localized creep process) serves to increase the conservatism of the design and assessment using the linear fracture mechanics methodology with room temperature fracture toughness values (a practical minimum toughness for the proposed application).

9.2 Recommendations

The results of Phases I, II, and III of the INEL support work provide a sound basis for a methodology to assure adequate quality of ceramic components to be used in structural applications, and to assess the remaining lifetime of in-service components and systems. The recommended methodology for quality assurance applies the concepts of linear elastic fracture mechanics, suitable stress intensity calibration equations, results of standardized material toughness property tests, and design stress states. Using this methodology, a design-allowable crack size can be determined. The developed NDE techniques can then be applied to the construction materials to ensure they will not fail in service due to pre-existing defects. If necessary, the same methodology can be applied in a different approach to determine safety or suitability to remain in service. Defects found during in-service inspections can be sized using NDE techniques. The defect size is used, along with the

operating conditions, to see if the design allowable stress intensity factor is being approached or exceeded.

The test results obtained in this work indicate that the fracture toughness values obtained from room temperature tests of mechanically notched (by EDM or diamond machining) specimens can be used to provided a conservative estimate of servicability over the range of temperatures expected in operation. Special preparation of test specimens to provide sharp-tipped precracks is not required, as this appears to artificially elevate the measured fracture toughness. Testing at elevated temperatures is not required, since no degradation of fracture toughness was observed. Using room temperature values will serve to provide a small amount of conservatism in the results of the analysis.

9. REFERENCES

Bar-On, I., Beals, J. T., Leatherman, G. L., and Murray, C. M. (1990), "Fracture Toughness of Ceramic Precracked Bend Bars," *J. Am. Ceram. Soc.*, **73**(8), pp. 2519-2522.

Baratta, Francis I. (1988), "Crack Stability in Two Brittle Nonmetallic Beam Systems," *Experimental Mechanics*, **28**(3), pp. 310-314.

Chuang, T.-J. and Wiederhorn, S. M. (1988), "Damage-Enhanced Creep in Siliconized Silicon Carbide: Mechanics of Deformation," *J. Am. Ceram. Soc.*, **71**(7), pp. 595-601.

Chuang, T.-J., Liu, W.-J., and Wiederhorn, S. M. (1991), "Steady-State Creep Behavior of Si-SiC C-Rings," *J. Am. Ceram. Soc.*, **74**(10), pp. 2531-2537.

E 399-90 (1991), "Standard Test Method for Plane-Strain Fracture Toughness of Metallic Materials," ASTM Designation E 399-90, **Vol. 3.01**, *1991 Annual Book of Standards*, Philadelphia, pp. 485-515.

E 813-89 (1991), "Standard Test Method for JIc, A Measure of Fracture Toughness," ASTM Designation E 813-89, **Vol. 3.01**, *1991 Annual Book of Standards*, Philadelphia, pp. 713-727.

Fujii, Toshimitsu and Nose, Tetsuro (1989), "Evaluation of Fracture Toughness for Ceramic Materials," *ISIJ Intl.*, **29**(9), pp. 717-725.

Gross, B. and Srawley, J. E. (1965), *Stress Intensity Factors for Three-Point Bend Specimens by Boundary Collocation*, NASA TN D-3092, National Aeronautics and Space Administration.

Hockey, B. J. and Wiederhorn, S. M. (1989) *Effect of Microstructure on the Creep of Reaction-Bonded Silicon Carbide*, National Institute of Standards Report, September 11, 1989.

Kunerth, D. C., Walter, J. B., and Telschow, K. L. (1987), *Nondestructive Evaluation of Silicon Carbide Heat Exchanger Tubes*, EGG-SD-7563, EG&G Idaho, Inc., April 1987.

Kunerth, D. and Johnson, J. (1987), *Utilization of Gaussian Ultrasonic Beam Calculations to Optimize Transducer Design for Tube Inspection*, SE-D-87-001, EG&G IIdaho, Inc., May 1987.

MIL-STD-1942A (1983), "(Proposed) Flexural Strength of High Performance Ceramics at Ambient Temperatures," November 1983, Department of the Army, Washington, D.C.

Newman, J. C. and Raju, I. S. (1979), *Stress Intensity Factors for the Surface Crack in a Finite Plate Under Tension or Bending Loads*, NASA TP 1578, December 1979.

Nose, Tetsuro and Fujii, Toshimitsu (1988), "Evaluation of Fracture Toughness for Ceramic Materials by a Single-Edge-Precracked-Beam Method," *J. Am. Ceram. Soc.*, **71**(5), pp. 328-333.

Post, D. (1987), "Moiré Interferometry," in *Handbook for Experimental Mechanics*, Ch. 7, Prentice-Hall, Philadelphia.

Reuter, W. G. (1986), *Applicability of Fracture Mechanics to Lifetime Prediction of B&W Ceramic Heat Exchanger Tubes*, EGG-MS-7451, EG&G Idaho, Inc., Idaho Falls, ID, November 1986.

Reuter, W. G., Lloyd, W. R., Knibloe, J. R., and Storhok, E. (1989), *Assessment of Strength Limiting Flaws in Ceramic Heat Exchanger Tubes, Phase II*, DOE/ID-10249, October 1989 (available from National Technical Information Service, Springfield, VA 22161).

Tada, H., Paris, P., and Irwin, G. (1973), *The Stress Analysis of Cracks Handbook*, Del Research Corp., Hellertown, PA, pp. 2.16-2.18.

Wiederhorn, S. M., Roberts, D. E., Chuang, T.-J., and Chuck, L. (1988), "Damage-Enhanced Creep in Siliconized Silicon Carbide: Phenomenology," *J. Am. Cer. Soc.*, 71(7), pp. 602-608.

APPENDIX A. ACOUSTIC EMISSION MONITORING

Acoustic emission (AE, sometimes called stress wave emission, or SWE) occur in solid materials during crack extension (AE is also generated by dislocation motion, but at much lower amplitudes). When an increment of crack growth occurs, an acoustic pulse (mechanical wave) is generated at the site, and radiates through the material. The initial wave may be multi-moded, and as the wave impinges on internal defects or free surfaces, additional mode conversion and wave guiding can occur. The resultant waveform is usually a combination of longitudinal, shear, and surface waves, each traveling at a different velocity. The frequency content of these waves are usually in the range 200 kHz to 1 MHz. By sonically coupling a suitable transducer to the material or test specimen, the AE generated by crack growth can be detected and recorded. A typical transducer uses a piezoelectric crystal to convert the elastic wave amplitude in the material to a corresponding low level electrical signal. This signal is then amplified and input to the AE system that detects and records the AE events.

The signals input to the acoustic emission monitoring equipment can be handled in various ways. Analog/digital hybrid (analog) systems usually detect the analog signal by using a voltage comparator to check the AE signal against a reference (or threshold) level. When the threshold level is exceeded, an AE event is recorded, and waveform parameters are measured via analog circuitry. Time, amplitude, and counting parameters that determine the envelope of the AE waveform are measured. The envelope parameters that are usually measured are depicted graphically in Figure 14. The envelope parameters are then recorded in digital format for each event. Relative times of event occurrence are also recorded. Other analog signals, corresponding to test parameters such as an applied force, pressure, or COD, can also be digitized and recorded. These parameters can be recalled and calculations can be done using them. Event energy is calculated by integrating the envelope and determining the enclosed area. The total area may be divided by $\sqrt{2}$ to account for the theoretical area swept by a purely sinusoidal waveform.

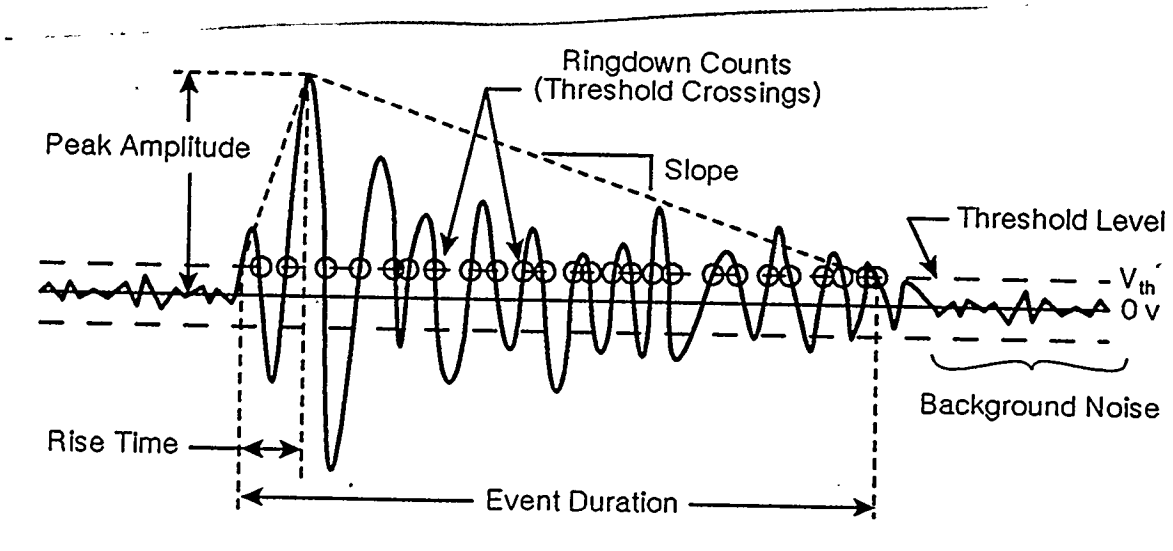

Figure 14. Schematic representation of an acoustic emission waveform showing characterizing parameters.

AE systems that are all digital operate differently. The preamplified analog electric signal that arrives at the system is continuously digitized by a loop-type analog-to-digital converter (ADC). A discriminator/comparator is used to detect the occurrence of an event. When an event occurs, the ADC is latched to capture the actual digitized waveform. This information is then transferred to digital storage (RAM, disk, or tape). Relative timing and the other converted (digitized) analog signals described above are also recorded. The waveforms can then be recalled and post-processed to determine the required information.

The two types of systems each have advantages and disadvantages. The analog systems can capture more events in a shorter period of time, but with less detail of the individual events. The analog system requires much less storage area to save its information. The digital-type system can record minute details of each event, but is restricted by digital data transfer rates. The digital system is therefore more limited to the number of events per unit time that it can record.

For general monitoring, the analog-type system provides more flexibility. The digital systems provide better support for certain, more specialized cases, such as precision source location or waveform analysis to differentiate event source types. An analog-type system, the AET 5500, was used for the monitoring of crack growth in this project.

APPENDIX B. SPECIMEN PREPARATION - GRINDING AND EDM

Generating Specimen Blanks from Tubular Sections

Rectangular bars of nominal dimensions 5 x 10 x 50 mm long were used in the testing program. These bars were fabricated from tube sections provided by B&W. Tube segments of 50 mm axial length were cut from the supplied tubes using a diamond-impregnated cutoff saw (Buehler Model 10-1000) with water-soluble oil as a coolant. These segments were then divided into 12 to 15 circumferential sectors with the same saw. The resulting sectors were then reduced to the final specimen dimensions by surface grinding parallel to the long axis of the specimen using a Bridgeport surface grinding machine, Model 815 (manual table feeds). A schematic diagram of the sectioning process is shown in Figure 15.

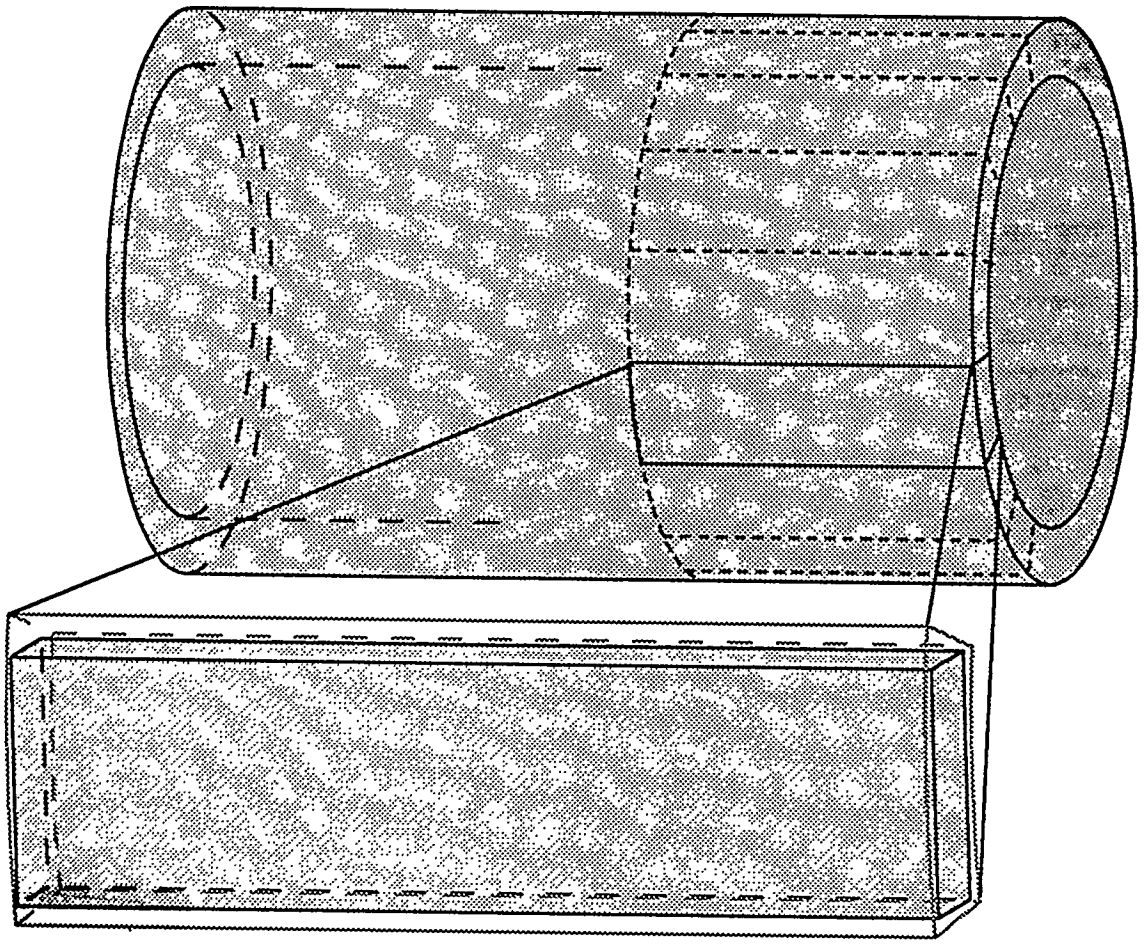

Figure 15. Segment of Si-SiC tube showing sectioning plan for removing SE(B) specimen blanks.

A 250 mm diameter diamond particle grinding wheel (Greenlee #401-010061-MDW-120-N-100-B-1/8) with 12.5 mm width operating at 1750 r.p.m. was used. The longitudinal feed rate was controlled manually with a moderately slow rate (estimated to be 30-60 mm/s). The crossfeed was about 2 mm/pass for stock removal and about 0.5 mm/pass for finishing to final dimensions. A water-soluble oil coolant was flooded over the specimen during all grinding. A maximum downfeed of 12.5 μm per pass was used during rough sizing of the bars. The final 100 μm of material on each surface was removed at a maximum downfeed of 4 μm per pass, with several passes made at zero downfeed to remove the last 4 to 6 μm of material. This sequence of grinding is an accepted method for preparing monolithic ceramic bend bars and is described in Section 5.1.4.3 of MIL-STD-1942A (1983), with the exception that the final grinding was not accomplished with a finer grit wheel. This omission was justified in that only testing with large cracks or notches was to be performed, and micro-damage of the specimen's surface would not have measurable influence on the test results, as it would in unnotched flexural strength tests which the MIL standard specifically addresses. The four long edges of each specimen did receive a 75-100 μm bevel at 45 degrees using a 600 grit diamond "file" (DMT Corp.). At this point the specimen blanks were ready for EDM notching or precracking as required.

EDM Notching of Specimen Blanks

Groups of 15 to 30 of the rectangular bars were sent to outside vendors[a] of electric discharge machining (EDM) services to have notches inserted. The notches were nominally 5 mm in length with a tip radius of 60 to 75 μm (65 μm specified). The notches were inserted using a computer-controlled, wire-type EDM system, with 125 μm diameter tantalum wire as the electrode. Details of current, dielectric medium, stock removal rate, and other process variables were not available from the service vendors. In the case of both vendors, the specimens had a discolored area (thought to be a thin oxide layer) that extended from the edge of the notch to a distance of 100 to 200 μm. It is surmised that this was the result of local heating during the machining process and that the EDM cutting was carried out in air (air used as the dielectric medium). The surface of the specimens in the vicinity of the EDM notch tip was examined using SEM, up to 4000x magnification, and no damage in the form of microcracking or microstructural change was visible. Examination under an optical microscope did not show any change in the general structure of the material in the same region.

The possible effects of any differences in the EDM process (although unknown, assumed to be very similar) used by the different vendors (process parameters were not available from either vendor) on the measured fracture toughness of the material were investigated by comparison testing three specimens made by each of the two vendors.[b] No statistically significant fracture toughness differences were detected in the tests. From these tests and observations it was determined that the different EDM vendors were providing equivalent test specimens, and that it was very unlikely that the EDM processing was having any detectable effect on the measured fracture toughness of the material.

---

a. Two vendors provided EDM services. EDM Laboratories, Inc., Santa Clara, CA, and Avtech Corp. (formerly Central Utah Tool), Provo, UT were used to place notches in separate lots of the bend specimens. EDM parameters used to notch the specimens were requested, but were not provided.

b. The effect of the EDM process on the material immediately surrounding the notch tip was addressed in Phase II of the program. Comparison of toughness data generated in Phase II with published data for similar Si-SiC materials showed no significant difference. It was decided then, that the EDM cutting process did not appreciably affect the materials fracture toughness.